

The University of Maine

DigitalCommons@UMaine

Electronic Theses and Dissertations

Fogler Library

Spring 5-2020

A Linear Actuator/Spring Steel-Driven Glove for Assisting Individuals with Activities of Daily Living

Daniel Chizhik

University of Maine, daniel.chizhik@maine.edu

Follow this and additional works at: <https://digitalcommons.library.umaine.edu/etd>



Part of the [Biomechanical Engineering Commons](#)

Recommended Citation

Chizhik, Daniel, "A Linear Actuator/Spring Steel-Driven Glove for Assisting Individuals with Activities of Daily Living" (2020). *Electronic Theses and Dissertations*. 3167.

<https://digitalcommons.library.umaine.edu/etd/3167>

This Open-Access Thesis is brought to you for free and open access by DigitalCommons@UMaine. It has been accepted for inclusion in Electronic Theses and Dissertations by an authorized administrator of DigitalCommons@UMaine. For more information, please contact um.library.technical.services@maine.edu.

**A LINEAR ACTUATOR/SPRING STEEL-DRIVEN GLOVE FOR ASSISTING
INDIVIDUALS WITH ACTIVITIES OF DAILY LIVING**

By

Daniel Chizhik

B.S. University of Maryland-Baltimore County, 2018

A THESIS

Submitted in Partial Fulfillment of the

Requirements for the Degree of

Master of Science

(in Mechanical Engineering)

The Graduate School

The University of Maine

May 2020

Advisory Committee:

Babak Hejrati, Assistant Professor of Mechanical Engineering, Advisor

Mohsen Shahinpoor, Professor of Mechanical Engineering

Andrew Goupee, Assistant Professor of Mechanical Engineering

**A LINEAR ACTUATOR/SPRING STEEL-DRIVEN GLOVE FOR ASSISTING
INDIVIDUALS WITH ACTIVITIES OF DAILY LIVING**

By Daniel Chizhik

Thesis Advisor: Dr. Babak Hejrati

An Abstract of the Thesis Presented
in Partial Fulfillment of the Requirements for the
Degree of Master of Science
(in Mechanical Engineering)

May 2020

Over three million people in the U.S. suffer from forearm and hand disabilities. This can result from aging, neurological disorders (e.g., stroke), chronic disease (e.g., arthritis), and injuries. Injuries to hands comprise one-third of all work-related injuries worldwide. This can lead to difficulties with activities of daily living (ADL), where one needs to grasp, lift, and release objects in the household. There is a rise in demand for assistive orthoses and gloves that can allow many people to regain their grasping/releasing ability and, thereby, their independence. The main contribution of this thesis is developing an assistive glove with the actuating mechanism comprised of linear actuators and strips of spring steel to enable bidirectional motion of users' fingers during ADL. The target group of people to use this proposed actuation system was chosen to those who had only diminished hand grasping capabilities. There are already many different gloves in the market. Each one uses different methods of actuation and force transmission, as well as different control methods. These gloves were analyzed by looking at their actuation mechanisms, control systems, and the benefits and downfalls of each one.

Vigorous testing was conducted to choose the most effective components for the actuating mechanism. Then, an assistive glove was fabricated which included a control system box that could be easily worn on the forearm of the user. Tests were conducted on the glove to test its effectiveness when the user's hand was completely passive using four to six participants. Motion capture, force, and electromyography (EMG) data were collected and from those, range of finger motion, maximum grasping capabilities, maximum force generation, and muscle activity were analyzed. The glove was shown to actuate the fingers enough to grasp objects with different sizes ranging in diameter from 40mm to 80mm, with maximum possible weight able to be picked up being around 1000g for the larger sizes. The glove could generate 4N-5N to the index and middle fingers and 10N to the thumb. EMG analysis showed that using the glove to pick up heavy objects caused a decrease in muscle activity of up to 80%. From this analysis, it was shown that the glove has potential to assist with ADL and would provide greater independence for those with diminished hand grasping abilities.

TABLE OF CONTENTS

LIST OF TABLES.....	iv
LIST OF FIGURES.....	v
Chapters	
1 INTRODUCTION.....	1
1.1 Current Actuation Designs	1
1.1.1 Methods of Actuation	1
1.1.2 Force Transmission.....	2
1.1.3 Control System Design.....	4
1.2 Sensors	6
1.2.1 EMG	6
1.2.2 Force Sensor	7
1.2.3 Flex Sensor	7
1.2.4 Distance Sensor	8
1.3 Biomechanics and Anatomy of the Human Hand and Forearm	9
1.3.1 Anatomical Directions.....	10
1.3.2 Bones and Joints.....	10
1.3.3 Muscles	11
2 PLAN OF ACTION FOR THE DESIGN OF THE GLOVE.....	13
2.1 Glove Objectives	13
2.2 Glove Part Selection	15
2.3 Finalized Glove Design Feasibility Testing	17
3 EXPERIMENTAL PROCEDURE	18
3.1 Actuation Mechanism Feasibility Test.....	18
3.2 Assessment of the Assembled Glove	21

3.2.1 Assembled Glove Motion Capture	21
3.2.2 Assembled Glove Grasping and Lifting Tests	22
3.2.3 Assembled Glove Force Generation Test	23
3.2.4 Assembled Glove Muscle Activity Test	24
4 RESULTS.....	29
4.1 Actuation Mechanism Feasibility Results.....	29
4.1.1 Steel Thickness	31
4.1.2 Actuator Type	33
4.1.3 Other Effects	35
4.2 Resulting Assistive Glove Design	37
4.3 Assessment of the Assembled Glove's Performance	42
4.3.1 Glove Assembly	42
4.3.2 Assembled Glove Motion Capture Results	43
4.3.3 Assembled Glove Grasping and Lifting Results.....	47
4.3.4 Assembled Glove Force Generation Results	49
4.3.5 Assembled Glove Muscle Activity Analysis.....	51
5 CONCLUSION	54
5.1 Possibilities for Future Investigation	55
REFERENCES.....	57
APPENDIX	62
BIOGRAPHY OF THE AUTHOR	65

LIST OF TABLES

Table 2.1	Technical information about the linear actuators [38], [39]	15
Table 3.1	DH Parameters. Lengths are in mm; angles are in radians (* indicates a variable).....	21
Table 4.1	Pairwise comparison of different masses affecting the dependent variables (* indicates a significant difference between pairs)	36
Table 4.2	Cost breakdown of the assistive glove. (~ indicates an estimated cost as it depends on where the parts are printed)	42
Table 4.3	Index finger lengths of each subject and their respective glove sizes	44
Table 4.4	The average angles of the live index finger and gloved index finger at maximum flexion along with their respective standard deviations	47
Table 4.5	Average percent differences, standard deviation, and pairwise comparison of the glove affecting muscle activity (* indicates a significant difference between the pairs).....	53

LIST OF FIGURES

Figure 1.1	Examples of different actuators used in orthosis and glove design: (a) DC motors [4], (b) a linear actuator [5], and (c) pneumatics [6]	2
Figure 1.2	Examples of a cable-driven mechanism by (a) In, et al. [10], (b) Nycz, et al. [11], and (c) Biggar, et al. [12]	2
Figure 1.3	Examples of high- and low-profile rigid linkages used in orthoses that were designed by (a) Wang, et al. [16], (b) Hasegawa, et al. [17], and (c) Ben-Tzvi, et al. [18]	3
Figure 1.4	Examples of soft robotic gloves by (a) Borboni, et al. [23], (b) Polygerinos, et al. [22], and (c) Gerez, et al. [24].	3
Figure 1.5	Examples of wearable control systems mounted on the (a) upper arm [3], (b) wrist [8], and (c) again on the upper arm [25]	4
Figure 1.6	Gloves designed by (a) In, et al. [26] and (b) Polygerinos, et al. [27] being controlled with a GUI	4
Figure 1.7	(a) A low-profile cable-driven glove and (b) its control system with attached actuators [13]	5
Figure 1.8	(a) A glove that uses a water pump to actuate the fingers and (b) its wearable control system [20]	5
Figure 1.9	(a) A control box with button control on its top. The microcontroller and pump parts are housed inside. (b) A glove with its control box (center) and GUI (left) [6], [28].	6
Figure 1.10	Examples of (a) a wet EMG and (b) a dry one	7
Figure 1.11	Examples of (a) an FSR, (b) a capacitive force sensor, and (c) a load cell [29]-[31]	7
Figure 1.12	(a) A flex sensor and (b) a glove that uses one in its control system [1]	8
Figure 1.13	Examples of (a) an ultrasonic sensor and (b) an IR sensor. (c) shows an assembled glove with the IR sensor located on the palmar side of the wrist [1]	9
Figure 1.14	A hand (a) grasping a coffee mug and (b) pinch gripping a pen	9
Figure 1.15	Anatomical directions of the hand and forearm	10
Figure 1.16	Joints of the hand	11
Figure 1.17	Posterior views of the muscles that control finger movement (a) Flexor digitorum superficialis, (b) flexor digitorum profundus, (c) extensor indicis, (d) extensor digiti minimi, and (e) extensor digitorum [37]	12

Figure 1.18	Posterior views of the muscles that control thumb movement. (a) Flexor pollicis longus, (b) abductor pollicis longus, (c) extensor pollicis brevis, and (d) extensor pollicis longus [37].	12
Figure 2.1	(a-b) The linear actuator-spring steel driven glove and (c) an up-close look at its actuating mechanism [38], [39].	14
Figure 2.2	The designed one-finger experimental setup	16
Figure 3.1	(a-b) Incremental extension of the linear actuator. (b) The placement of tracking markers in Tracker	19
Figure 3.2	Kinematic diagram of the finger	20
Figure 3.3	A diagram of the DH frames attached to the actuation mechanism in a zero-angle position	20
Figure 3.4	Examples of common household objects. (a) a jar of pasta sauce, a water bottle, and a speaker. (b) a tube of lotion	22
Figure 3.5	The container used for testing (far right) and the different caps. From left to right, the cap diameters are 40mm, 50mm, 60mm, 70mm, and 80mm. The container is also 80mm in diameter	22
Figure 3.6	The force testing setup with the FSR attached to the side of the cylinder. The microcontroller is on the bottom left	23
Figure 3.7	Calibration curve for the FSR used in the experiment	24
Figure 3.8	The muscles used in the experiments. (a) ECRL, (b) FCR, and (c) FDS [47]	25
Figure 3.9	Anterior (a,d), lateral (b,e), and posterior (c,f) views of extensor and flexor muscles. (a)-(c) show the finger extensor and flexor muscles overlapping over each other and (d)-(f) show the muscles that the EMGs were positioned over [37].	26
Figure 3.10	(a) The collected MVC signal of the extensor carpi radialis longus. (b) shows the muscle from the anterior side and (c) shows it from the lateral side [48].	27
Figure 3.11	Plot of filtered muscle signal (a) before resting signal is subtracted, and (b) after. The shaded areas are what were integrated.	28
Figure 4.1	Graphical representation of the workspace of the actuation mechanism (blue "o") and the fingertip coordinates (red "x"). The left y-axis shows the shim's height from the forward kinematics analysis, while the right y-axis shows the height of the fingertip from motion capture analysis	30
Figure 4.2	Finger joints' heights when using the L12 actuator with (a) no load, (b) 100g, (c) 300g, and (d) 400g. Solid lines represent the 0.010" strip while the dashed lines represent the 0.025" strip. The vertical dashed lines indicate the stroke increments. The profiles for different masses using the L16 actuator follow similar patterns.	31

Figure 4.3	Joint angles of the model finger under the L12 actuator, 0.010" strip, while lifting a 300g mass. Solid lines represent the 0.010" strip and dashed lines represent the 0.025" strip. The vertical dashed lines indicate the stroke increments. Similar behavior was observed when using the L16 actuator, or when using heavier masses.....	32
Figure 4.4	Bar plots show the means and standard errors of the fingertip height at the actuators' full extension for different (a) strip thicknesses and (b) masses (* indicates a significant difference between the conditions)	33
Figure 4.5	Bar plots show the means and standard errors of the extension and retraction velocities of both actuators and strips tested by different masses. The (a) L12 actuator with 0.010" strip, (b) L16 actuator with 0.010" strip, (c) L12 actuator with 0.025" strip, and (d) L16 actuator with 0.025" strip.....	34
Figure 4.6	Bar plots show the means and standard errors of the extension velocities. (a) Extension velocity and (b) retraction velocity for different actuator types and masses. The * indicates a significant difference between the conditions	35
Figure 4.7	Bar plots show the mean and standard errors of the tip height for both actuators and strips tested by different masses. The (a) L12 actuator with 0.010" strip, (b) L16 actuator with 0.010" strip, (c) L12 actuator with 0.025" strip, and (d) L16 actuator with 0.025" strip.....	36
Figure 4.8	The assembled assistive glove	37
Figure 4.9	The three different gloves available for users. (a) medium, (b) large, and (c) extra-large. The large glove has the actuating mechanism connected to it	38
Figure 4.10	(a) The control system hardware inside the housing and (b) the battery connected to the PowerBoost. (c) and (d) show the two different control mechanisms: a flex sensor inside a sleeve on the pinky finger and a control box	40
Figure 4.11	The fully assembled glove worn on the right hand with the flex sensor control option Implemented. (a) anterior view and (b) posterior view	41
Figure 4.12	The steel strip for the thumb being fixed to the thimble	43
Figure 4.13	Screenshots of the Tracker software for (a) a free-moving finger, (b) a cylinder, and (c) a finger freely actuated by the glove.....	44
Figure 4.14	Finger joint motion profiles of each subject while grasping a 40mm cylinder, 80mm cylinder, and nothing. The final plot (F) has the motion profile of Subject F grasping a 70mm cylinder instead because that was the largest object he could grasp	45
Figure 4.15	The finger joint motion profiles of (a) a 40mm cylinder, (b) an 80mm cylinder, and (c) free movement when Subject B is wearing the glove and when he isn't. The point in the lower left-hand part of each plot is the stationary MCP joint and the rightmost profiles are those of the fingertip	46

Figure 4.16	Joint angles of the index finger when the glove is not used (blue) and when it is used (red).....	47
Figure 4.17	The experiment being conducted with a subject attempting to grasp (a) a 70mm cylinder and (b) a 40mm cylinder	48
Figure 4.18	Liftable weight in relation to the size of the cylinder	49
Figure 4.19	A subject grasping the 80mm cylinder with the FSR collecting force data from the middle finger	50
Figure 4.20	Force generated by each digit on the cylinder	50
Figure 4.21	The EMG acquisition software running on the computer and the subject getting ready to lift the cylinder.....	51
Figure 4.22	Muscle activity of the FDS of Subject B (a) when the glove was not used and the hand was active, and (b) when the glove was used and the hand was passive	52
Figure 4.23	(a) Average muscle activity while the cylinder was manipulated. (b) Percent decrease in muscle activity between the case of lifting an object with and without the glove.....	52
Figure A.1	Design iterations of the dorsal actuator mount.....	62
Figure A.2	Design iterations of the thumb actuator mount	62
Figure A.3	Design iterations of the thimbles. Model v3 was used in the initial feasibility test	63
Figure A.4	Design iterations of the control system box	63
Figure A.5	Design iterations of the spring steel strips	64

CHAPTER 1

INTRODUCTION

Over three million people in the U.S. suffer from forearm and hand disabilities. This can result from aging, neurological disorders (e.g., stroke), chronic disease (e.g., arthritis), and injuries. Injuries to hands comprise one-third of all work-related injuries worldwide [1]. This can lead to difficulties with activities of daily living (ADL), where one needs to grasp, lift, and release objects in the household. There is a rise in demand for assistive orthoses and gloves that can allow many people to regain their grasping/releasing ability and, thereby, their independence [2], [3].

The following sections in this chapter will go over the current advances in orthosis design. Various actuation and sensing mechanisms will be discussed in this chapter. Different control strategies will be reviewed, and a brief explanation of the biomechanics of a human hand and its anatomy will also be covered.

1.1 Current Actuation Designs

1.1.1 Methods of Actuation

Robotic gloves are comprised of three parts: actuators, a method by which to transmit the force from the actuator to the fingers, and a control system. The most commonly used actuators are DC motors, servo motors (rotary or linear), and pneumatics. Examples of orthoses and gloves using the different actuators are shown in Figure 1.1. Figure 1.1(a) shows an orthosis that uses DC motors to actuate rigid linkages, whereas Figure 1.1(b) utilizes a linear actuator to move cables. Figure 1.1(c) uses pneumatic actuators to send air through tubes along the fingers to actuate them.

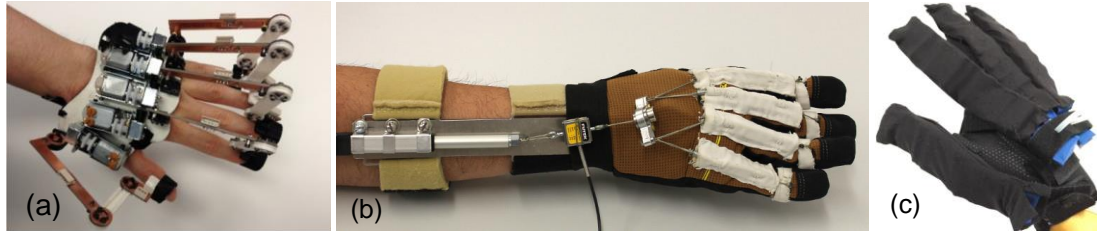


Figure 1.1 Examples of different actuators used in orthosis and glove design: (a) DC motors [4], (b) a linear actuator [5], and (c) pneumatics [6].

1.1.2 Force Transmission

The most commonly used forms of force transmission from the actuators to the fingers are with cables, rigid linkages, or tubing. Each method of force transmission has its advantages and disadvantages.

Cable-driven gloves can have a very low profile on the hand and very effective in manipulating a wide variety of objects [1], [7]-[9]. They allow the user to have as much of a range of motion in the hand as a healthy person. Depending on how they're designed, these gloves may provide unidirectional or bidirectional movement of the fingers. However, the cables are at risk of getting jammed in the cable guide, which leads to insufficient force transmission to the fingertips. Figure 1.2 shows different examples of cable-drive gloves.

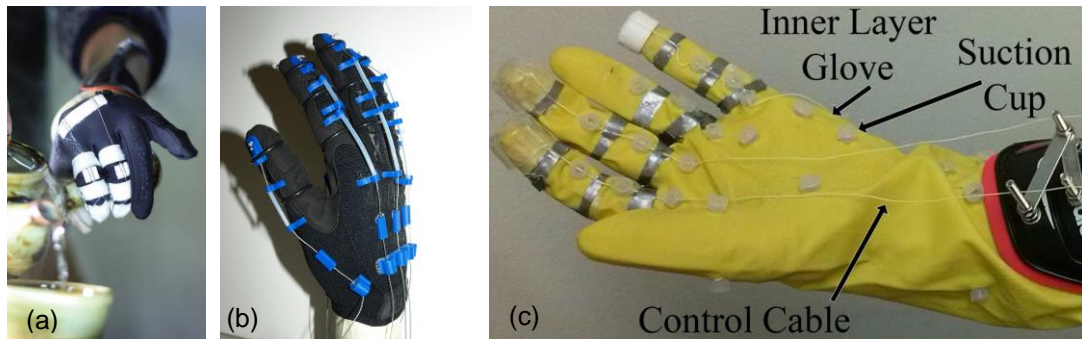


Figure 1.2 Examples of a cable-driven mechanism by (a) In, et al. [10], (b) Nycz, et al. [11], and (c) Biggar, et al. [12].

Rigid linkages are another effective method for actuating each finger. These methods have been used designs by Cui, et al. [13], Ho, et al. [14], and Arata, et al. [15], to name a few. However, if the linkages are too big, which they are in many cases, they

can restrict the user's ability to grasp certain objects such as things with handles (e.g., mugs, kettles, and coffee pots). Having linkages for each finger also increases the complexity of the orthosis and has an increased risk of something going wrong during operation such as the linkage joints misaligning. Figure 1.3 shows examples of different rigid linkage designs.

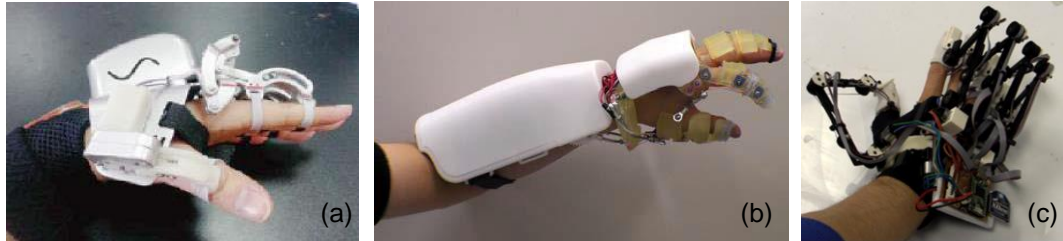


Figure 1.3 Examples of high- and low-profile rigid linkages used in orthoses that were designed by (a) Wang, et al. [16], (b) Hasegawa, et al. [17], and (c) Ben-Tzvi, et al. [18].

Gloves that use pneumatics require tubing to transfer force to the fingertips, such as those made by Yap, et al. [19], Polygerinos, et al. [20], and Connelly, et al. [21]. These tubes are usually used to inflate special pockets that sit along the fingers. As fluids are pumped into them, the inflated pockets curl the fingers. This is a very effective and low-profile way of actuating hands. Unfortunately, the air compressors and fluid pumps used in these designs can be bulky, heavy, and noisy, restricting the portability of the glove. Figure 1.4 shows different examples of gloves that implement pneumatics to actuate the fingers.

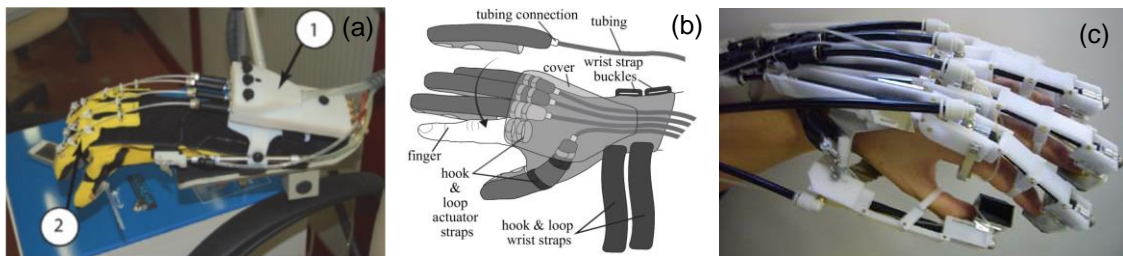


Figure 1.4 Examples of soft robotic gloves by (a) Borboni, et al. [22], (b) Polygerinos, et al. [23], and (c) Tadano, et al. [24].

1.1.3 Control System Design

As previously stated, size matters when it comes to the design of a glove, and that does not change for the control system hardware. A compact control box, such as the ones in Figure 1.5, will allow the user to use the glove more easily and in a greater number of places.

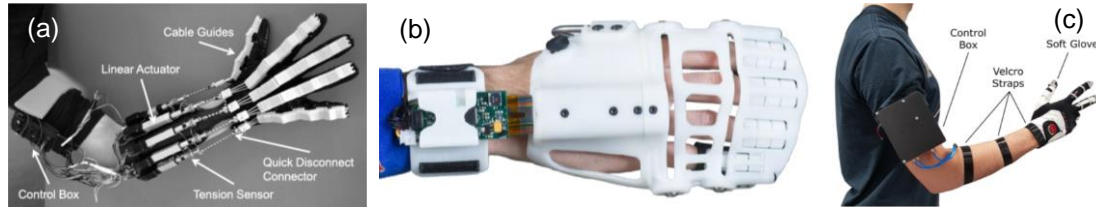


Figure 1.5 Examples of wearable control systems mounted on the (a) upper arm [3], (b) wrist [8], and (c) again on the upper arm [25].

Control systems are made up of a power source, some sort of circuit board, such as a microcontroller or even a graphical user interface (GUI), and any other electrical components associated with controlling the gloves' actuation, such as sensors. If the control system uses a GUI, such as those in Figure 1.6, the glove is usually intended for feasibility testing or rehabilitation and not everyday use.

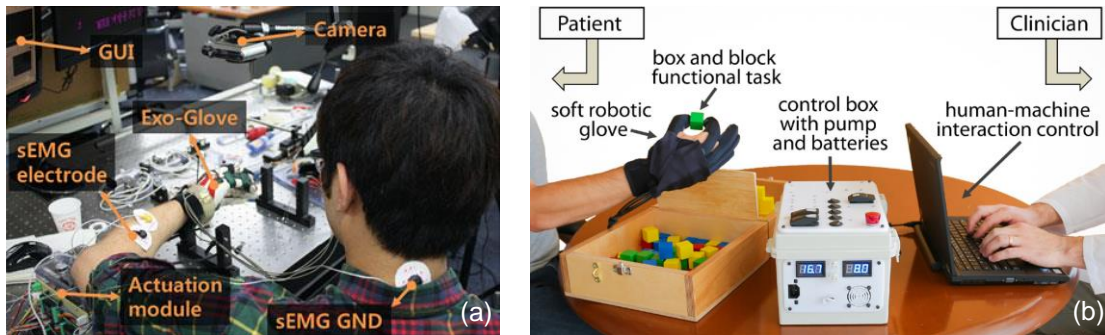


Figure 1.6 Gloves designed by (a) In, et al. [26] and (b) Polygerinos, et al. [27] being controlled with a GUI.

Depending on the overall design of the glove, the actuators may be housed with the control system. The cable-driven glove by Cui, et al. shown in Figure 1.7 is low-profile and very effective for ADL [13]. However, the control system and actuators are not wearable, limiting the portability of the device.

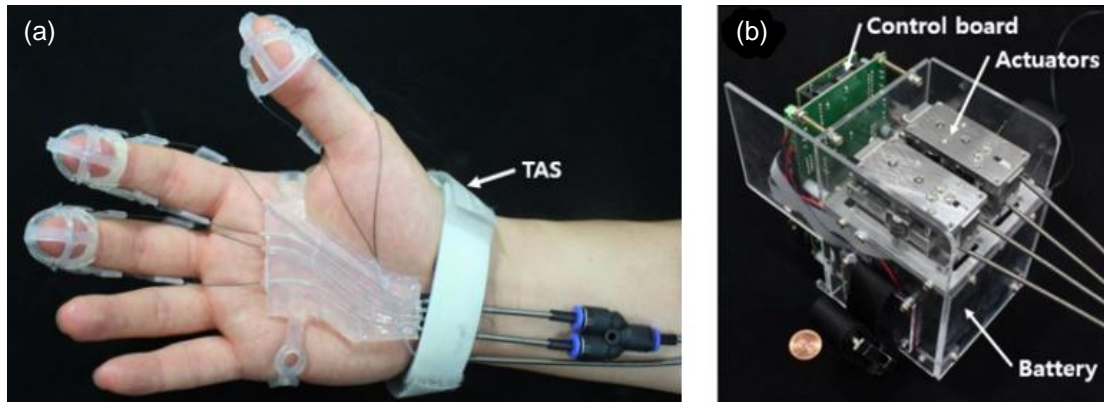


Figure 1.7 (a) A low-profile cable-driven glove and (b) its control system with attached actuators [13].

Similarly, gloves with air compressors and hydraulic pumps suffer from the lack of portability. The control system itself may be small, but the air pump and its additional components are housed with it as shown in Figure 1.8(b). The entire system has been designed to be worn on the waist but would still be difficult to don without assistance.

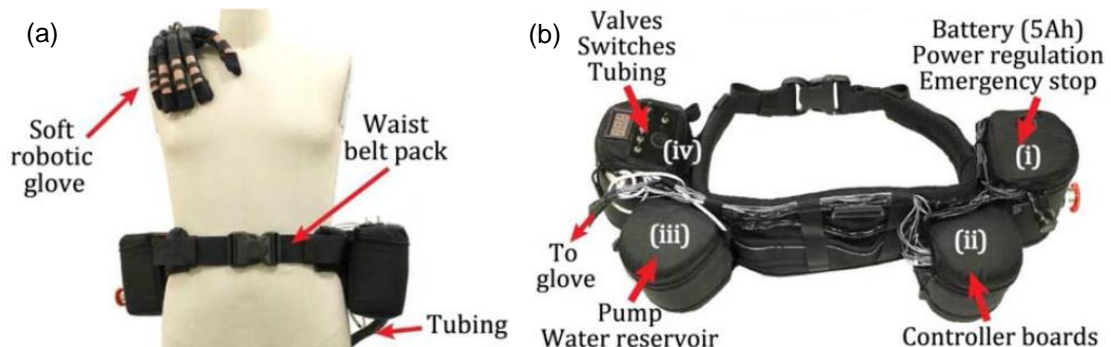


Figure 1.8 (a) A glove that uses a water pump to actuate the fingers and (b) its wearable control system [20].

If the control system does not use any sensors on the glove, buttons located on the control box may be used, as shown in Figure 1.9. It is important to note that these gloves are mainly intended for rehabilitation, so it is not critical for the control box to be easily transportable. However, the fact remains that a compressed air-based control system is not the best option for having a lightweight and portable glove.

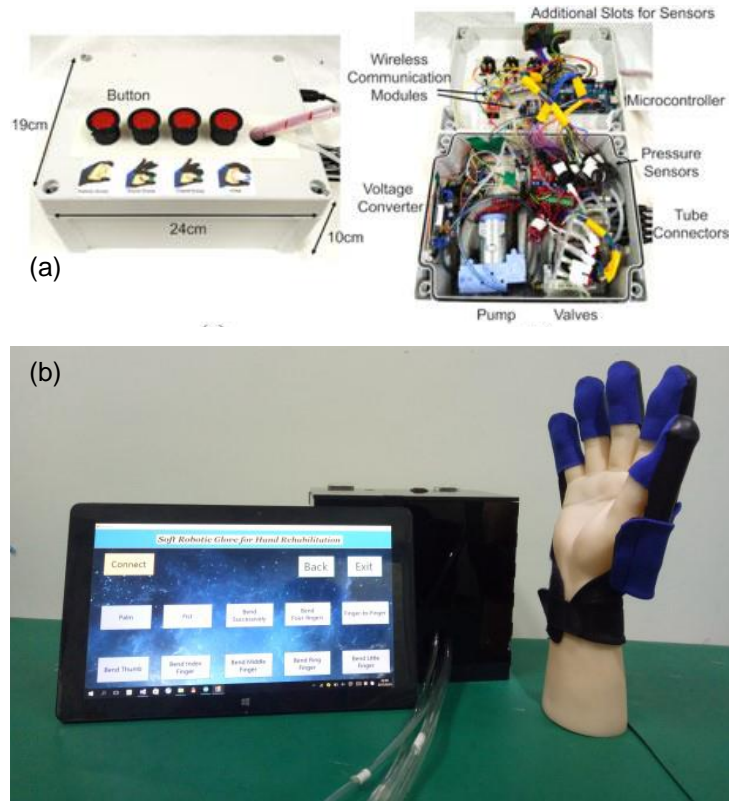


Figure 1.9 (a) A control box with button control on its top. The microcontroller and pump parts are housed inside. (b) A glove with its control box (center) and GUI (left) [6], [28].

1.2 Sensors

Sensors are used in different ways in a control system. They may be used as inputs to actuate the glove or feedback sensors. Electromyography (EMG), force, flex, and distance sensors are such examples.

1.2.1 EMG

EMG sensors are used to measure the muscle activity as a means of controlling an glove. The higher the voltage measured, the higher the muscle activity. The most common type of EMG used in control systems are surface EMGs (EMG). These sit on one's skin using an adhesive. They use either an electroconductive adhesive membrane (called wet EMG) or metal contacts (called dry EMG) to detect the muscle activity.

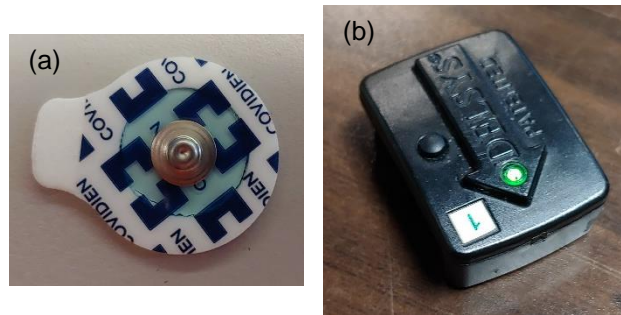


Figure 1.10 Examples of (a) a wet EMG and (b) a dry one.

1.2.2 Force Sensor

Two kinds of force sensors are typically used in control systems: a resistance-based sensor called a force sensitive resistor (FSR), or a capacitive-based sensor. These sensors measure the change in either resistance or capacitance. As the applied force increases, the value the sensors read increases. Another type of force sensor, called a load cell, may also be used, but they are usually only used to test the glove and not control it. The following figure shows examples of each force sensor.

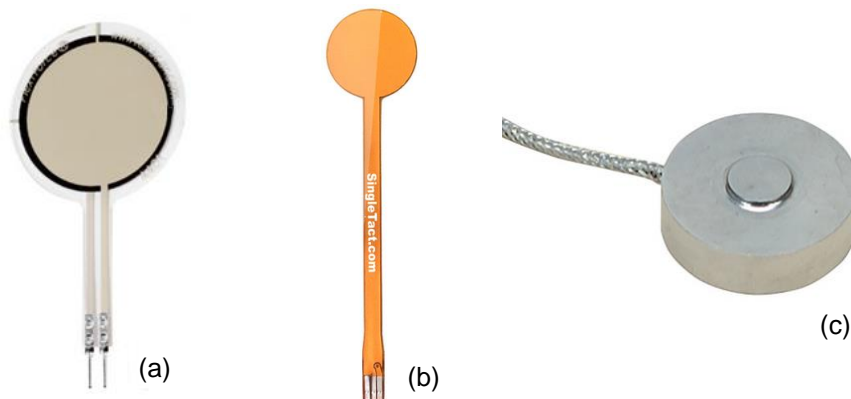


Figure 1.11 Examples of (a) an FSR, (b) a capacitive force sensor, and (c) a load cell [29]-[31].

1.2.3 Flex Sensor

Flex sensors act the same way as FSRs in the sense that they read the change in resistance, this time by the sensor's bending. As the sensor bends more, the resistance increases. Because flex sensors are long and thin, they can be attached to one or more fingers in a glove to independently control them. Figure 1.12 shows an

example of a flex sensor and a glove design by Popov, et al. that uses one its control system [1].

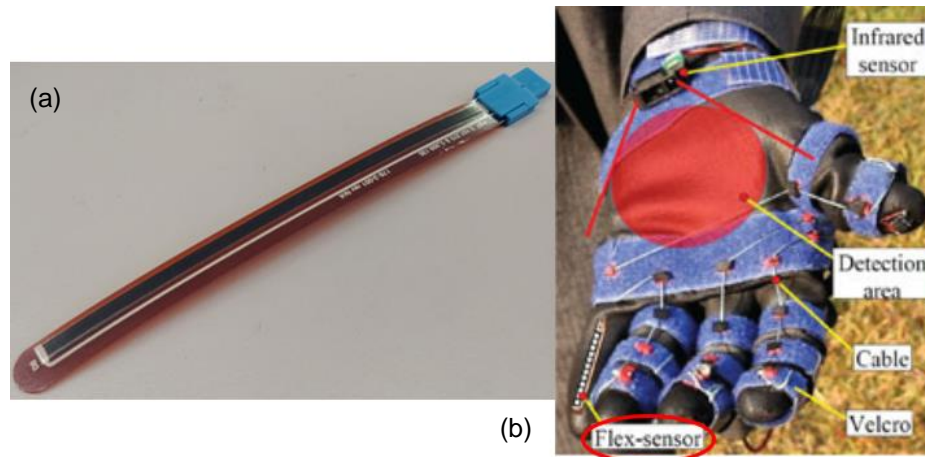


Figure 1.12 (a) A flex sensor and (b) a glove that uses them in its control system [1].

Flex sensors may also be calibrated like FSRs to measure the angle of something bending, like a finger joint. This is done by collecting the analog output signal of the sensor when it is bent at different angles. The data is then analyzed the same way as the FSR data to find an equation that relates analog signal to angle measurement.

1.2.4 Distance Sensor

A distance sensor may be attached to the palmar area of a glove to detect when it is close enough to an object to grasp it. One such sensor uses ultrasound to detect a change in distance, but these are rather large. A more low-profile sensor is an infrared (IR) sensor. This one uses a small infrared light to detect a change in distance. Figure 1.13 shows examples of (a) an ultrasonic sensor, (b) an IR sensor, and (c) a glove that uses a distance sensor in its control system.

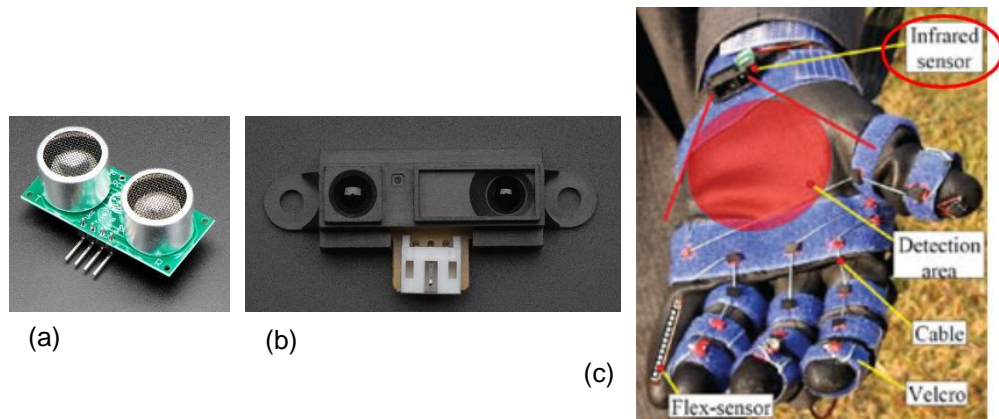


Figure 1.13 Examples of (a) an ultrasonic sensor and (b) an IR sensor. (c) shows an assembled glove with IR sensor located on the palmar side of the wrist [1].

1.3 Biomechanics and Anatomy of the Human Hand and Forearm

From a mechanical standpoint, the anatomy of the hand is the most complex part of the human body. It is our main way of interacting with the environment, and its dexterity allows us to manipulate different tools and objects. Positioning the fingers differently allows us to grasp large objects and perform a pinch grip on smaller objects. Diminished grip strength can be caused by illness, such as stroke or arthritis, or injury, such as a spinal injury.

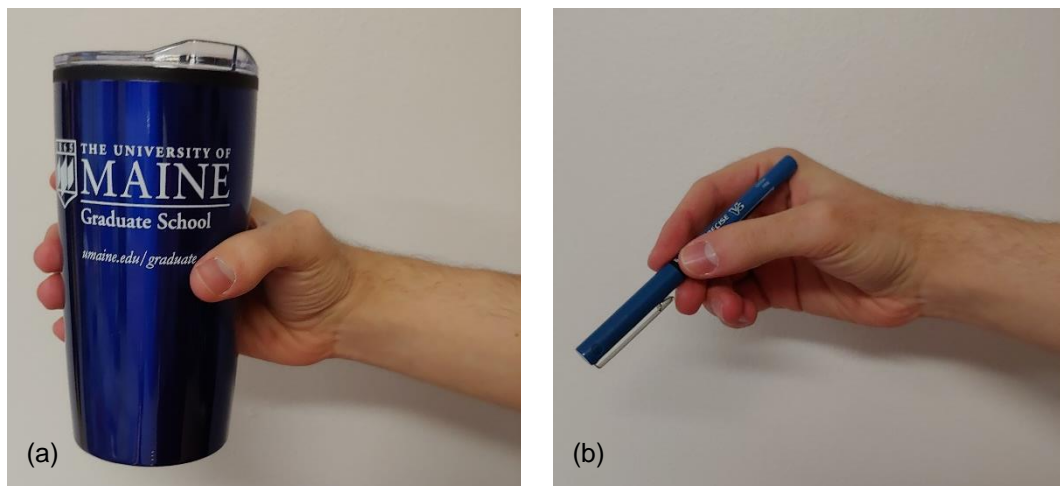


Figure 1.14 A hand (a) grasping a coffee mug and (b) pinch gripping a pen.

1.3.1 Anatomical Directions

Directions are important when discussing any part of human anatomy. The terms vary depending on what part of the body is being referred. For the hand, the following directional terms are used [32]. Moving from the wrist to the fingers is called the distal direction. Moving vice versa is called the proximal direction. The direction towards the thumb from the imaginary midline of the hand is called lateral and the direction towards the pinky finger from the midline is called medial. The palm's side of the hand is called the palmar side and the opposite side is called the dorsal side. Moving towards the palm is called the anterior direction and moving towards the dorsal side is called the posterior direction.

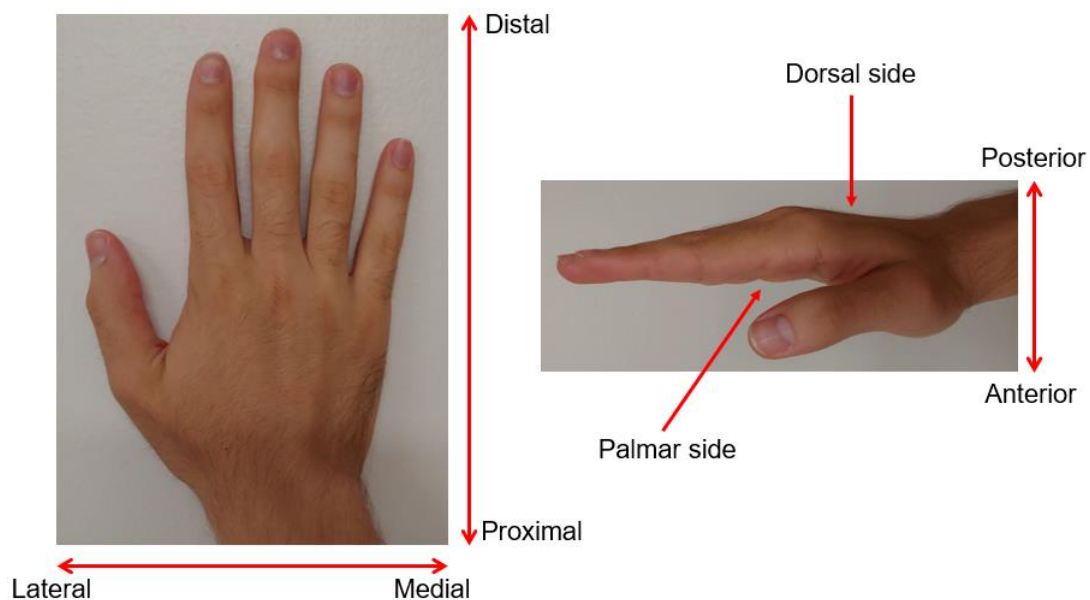


Figure 1.15 Anatomical directions of the hand and forearm.

1.3.2 Bones and Joints

Each digit in the hand is comprised of three joints [33], as shown in Figure 1.16. The joint closest to the palm is called the metacarpophalangeal joint (MCP). The next joint is called the proximal interphalangeal joint (PIP). The last one is called the distal interphalangeal joint (DIP). The joints are a bit different for the thumb. The farthest joint is just called the interphalangeal joint, but for simplicity, it shall be called the PIP here.

The next joint closer to the palm is the MCP. The joint closest to the wrist is called the carpometacarpal joint (CMC).

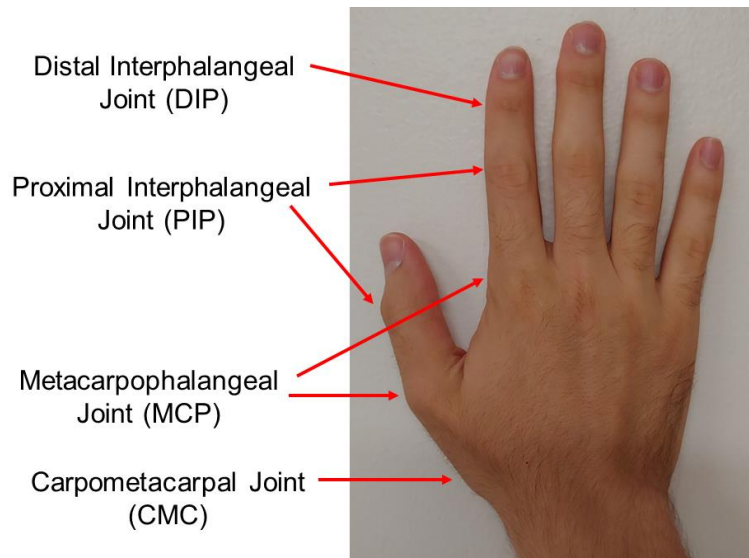


Figure 1.16 Joints of the hand.

1.3.3 Muscles

The muscles that control the movement of the fingers are located in the forearm. According to W. D. Gardner's *Structure of the Human Body*, there are five muscles that do this [34]. They are the flexor digitorum superficialis, flexor digitorum profundus, extensor digitorum, extensor digiti minimi, and extensor indicis. As the names imply, the first two muscles control finger flexion and the last three control finger extension. Figures 1.17(a-b) show the flexor muscles and Figures 1.17(c-e) show the extensor muscles.

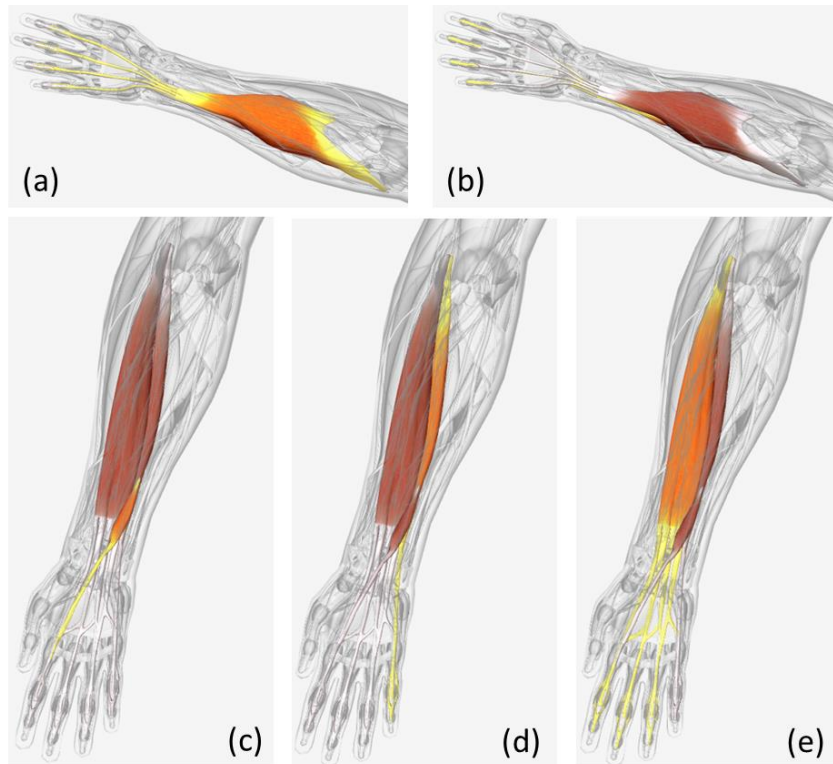


Figure 1.17 Posterior views of the muscles that control finger movement. (a) Flexor digitorum superficialis, (b) flexor digitorum profundus, (c) extensor indicis, (d) extensor digiti minimi, and (e) extensor digitorum [35].

An additional four muscles, shown in Figure 1.18, are used for controlling thumb flexion and extension. They are the flexor pollicis longus, abductor pollicis longus, extensor pollicis brevis, and extensor pollicis longus.

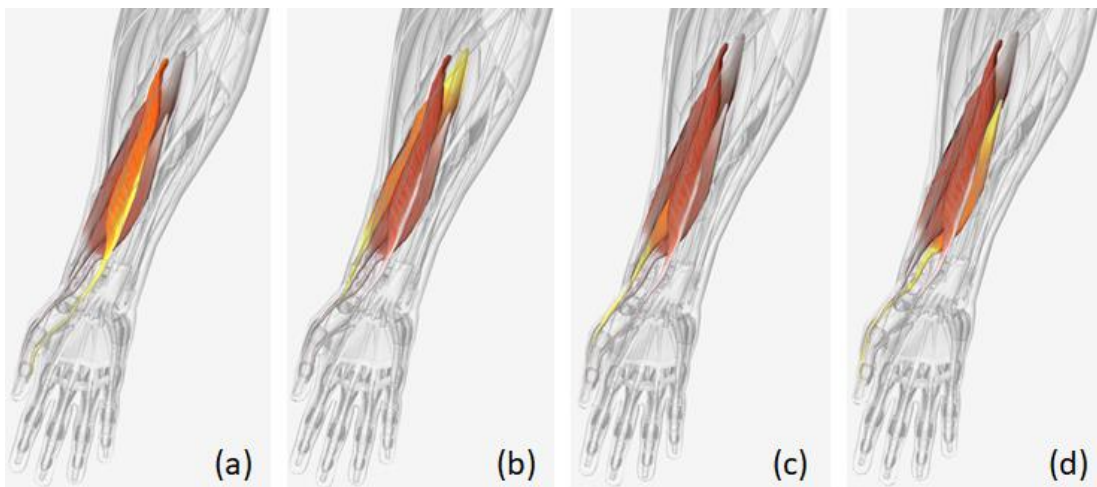


Figure 1.18 Posterior views of the muscles that control thumb movement. (a) Flexor pollicis longus, (b) abductor pollicis longus, (c) extensor pollicis brevis, and (d) extensor pollicis longus [35].

CHAPTER 2

PLAN OF ACTION FOR THE DESIGN OF THE GLOVE

The research conducted on different gloves yielded many different designs, each with their merits and downsides. In order to design a unique glove without any of the possible issues mentioned in the previous chapter, a different approach had to be taken. This chapter will discuss what the glove should be able to do, how the different parts of the glove will be chosen, and how the final design will be tested.

2.1 Glove Objectives

The goal of this research is to design a new glove that performs as well as the current designs already conceived of without any of the potential flaws. It should be intended for people who need assistance grasping household items. The glove will not be intended to fully replace a person's grasping capabilities.

Many gloves only actuated the index and middle fingers and the thumb while still transmitting enough force to assist with activities of daily living (ADL) [10], [25], [26]. Therefore, the new glove would also actuate these three digits. The proposed actuation mechanism design follows the idea of using spring steel for transferring force to the fingertips, as found in a number of papers [15], [36], [37].

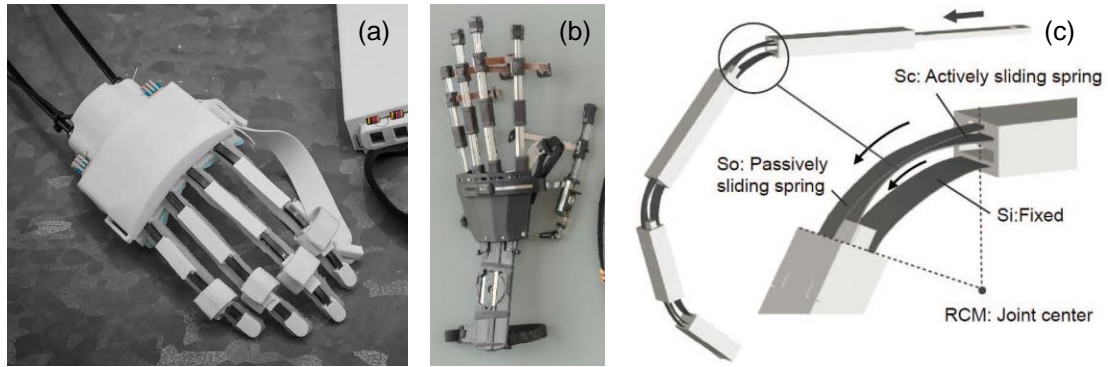


Figure 2.1 (a-b) The linear actuator-spring steel driven glove and (c) an up-close look at the actuating mechanism [36], [37].

As shown in Figure 2.1, this spring steel design was able to mimic the natural curling motion of the hand and was able to transmit 3N of force to each finger. The three layers of steel made the system act like a Bowden cable so that it could accommodate compression. Furthermore, it had no potential risks associated with cable-driven or rigid linkage force transmission methods. Investigation into this specific force transmission method had been done prior to this glove, so incorporating spring steel in this thesis seemed like an opportune way to further research its potential applications.

It has been noted that the grasping forces needed to manipulate objects in ADL are typically within the range of 10N-15N [1], [18], [20], [22]. The goal of this glove is to generate 3N-5N of force for each finger using this linear actuator/spring steel actuation system so that up to 15N of grasping force may be generated by using multiple actuators in the glove. Another goal of the proposed design would be to actuate the index and middle fingers and the thumb to enable both grasping and pinching tasks. This design can mitigate the issues of joint misalignment and cable management by directly moving the fingertip to enable grasping. Bidirectionality, or having the actuation mechanism both flex and extend the fingers, is another goal the glove should meet.

The design in Figure 2.1 uses three layers of spring steel to enable curling of a finger and transmit force to the fingertip. The proposed design in this thesis used a single strip of spring steel to transmit force directly to the fingertip by converting the

linear motion of the actuator to the bending motion of the finger. The proposed design is simpler than the one in Figure 2.1, which means the risk of faulty operation is decreased. The actuators were positioned on a base on the dorsal side of the hand with strips of spring steel extending from the actuators to the distal phalanx of each finger. The microcontroller and power source were positioned somewhere on the forearm in order for the entire system to be easily transportable.

2.2 Glove Part Selection

The parts of the glove were chosen through rigorous experiments. The 50-mm stroke Actuonix L12 and L16 actuator were chosen to be tested for the glove, where the L12 has been used by Ho, et al. [14]. These models were chosen for their lightweight, compact size, and easy-to-control features. Technical information about the actuators are found in Table 2.1.

Table 2.1 Technical information about the linear actuators [38], [39].

Actuator Type	L12	L16
Model Number	L12-50-50-6-R	L16-50-35-6-R
Gear Ratio	50:1	35:1
Retracted Dimensions (L x W x H)	102mm x 15.1mm x 18mm	118mm x 18mm x 20mm
Mass	40g	56g
Max. Generated Force	22N	50N
Max. No Load Speed at 6V	25mm/s	32mm/s

The spring steel used in the preliminary feasibility testing is AISI 1095 shim steel. One strip was 0.01” thick and the other was 0.025” thick. These thicknesses were chosen to serve as the limits of a range of possible thicknesses to use. Strips thinner than 0.01” were deemed too flimsy to be able to lift weight and those thicker than 0.025” were deemed to be unnecessarily rigid to allow flexibility with the design. The dimensions of the strips were 13mm wide and 73mm long. Cantilever buckling calculations were made which showed the stiffness of the 0.01” thick strip was 27.32N/m

and the stiffness of the 0.025" strip was 427.35N/m. This indicates that the thinner strip might not be as effective as the thicker one in actuating the finger.

The actuators and steel strips were tested using an experimental setup consisting of a 3D-printed mounting structure and model finger, the actuating system, and a hanging weight to evaluate the actuators' generated forces and motions. This setup enabled the quantification of performance of the actuators and strips rather than the user.

A 3D-printed thimble was also fabricated and positioned on the dorsal side of the distal phalanx to secure the steel strip onto the finger. The model finger simulated a user's passive finger for which the actuating system would provide full assistance. Although the model finger did not behave like a natural finger whose distal phalanx movement relies on the movement of the intermediate phalanx, it could still give an approximation of how an actual finger would behave with this system in place. The entire setup was constructed such that the model finger would curl upwards to lift various weights, as shown in Figure 2.2. The actuators would be controlled with an Arduino Uno microcontroller and powered by a 9V battery.

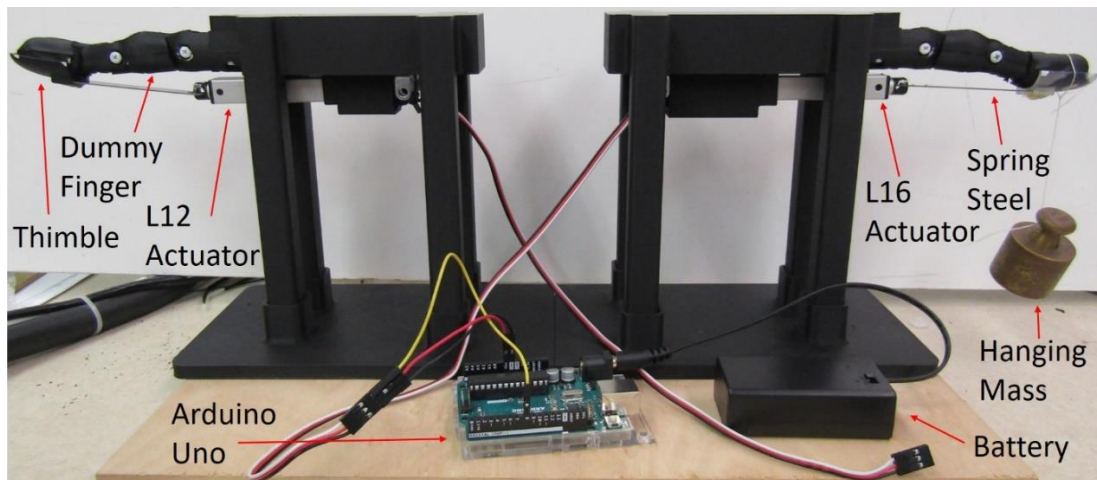


Figure 2.2 The designed one-finger experimental setup.

2.3 Finalized Glove Design Feasibility Testing

Once the glove has been fully assembled, further experiments were conducted to test the feasibility of the glove with human subjects, both healthy young adults and older adults. It has been shown that older people have a weaker hand grip strength, meaning they have to exert more energy during ADL than healthy people [40]. This is reflected in their muscle activity [41]. For this reason, muscle activity was measured in the human subjects to see if there was a noticeable change in the activity when the glove was being used to manipulate different sized and weighted objects versus when the subjects used solely their own abilities to perform the same tasks. Grasping force generated by the glove was also measured. Adjustments to the design of the assistive glove were made following analysis of the collected data and further experiments may be conducted.

CHAPTER 3

EXPERIMENTAL PROCEDURE

In order to prove the effectiveness of the designed glove, numerous tests had to be conducted. This chapter will discuss the feasibility experiments done for the actuating mechanism followed by the tests done on the fully assembled glove. The tests consisted of motion capture while attempting to grasp different sized objects, determining how much users are able to pick up with the glove depending on the size of the objects, force generation capabilities of the glove, and muscle activity analysis while the glove is being used.

3.1 Actuation Mechanism Feasibility Test

The Arduino microcontroller was programmed to extend the linear actuator in four quarter-stroke increments, 12.5mm, 25mm, 37.5mm, and 50mm, and retract it in the same way. This allowed for better analysis of the model finger's movement. The actuating system in Figure 2.2 was tested by adding hanging masses to the end of the finger with increments of 100g. Each mass was tested five times. Motion data in the form of x- and y-coordinates of the PIP and DIP joints, and the fingertip was then collected using Tracker Video Analysis software [42]. The MCP joint was stationary and served as the origin. Screenshots showing the different increments of the actuator extension with the tracking markers on each joint can be shown in Figure 3.1. This data was then exported into MATLAB to calculate the three joint angles.

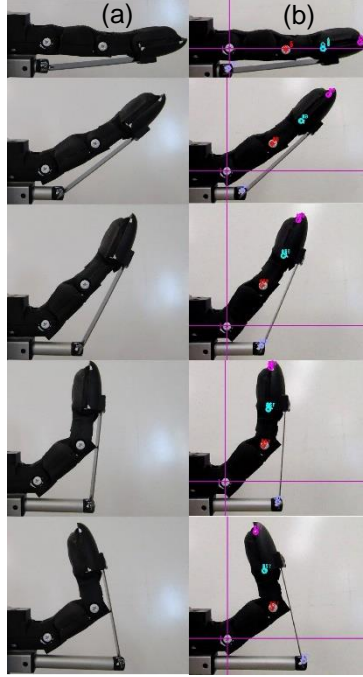


Figure 3.1 (a-b) Incremental extension of the linear actuator. (b) The placement of tracking markers in Tracker.

Using the joints' coordinates, vectors were formed between phalangeal joints as represented in Equations (1) – (3):

$$\mathbf{I}_{MCP} = \begin{bmatrix} PIP_x \\ PIP_y \end{bmatrix} \quad (1)$$

$$\mathbf{I}_{PIP} = \begin{bmatrix} DIP_x - PIP_x \\ DIP_y - PIP_y \end{bmatrix} \quad (2)$$

$$\mathbf{I}_{DIP} = \begin{bmatrix} Tip_x - DIP_x \\ Tip_y - DIP_y \end{bmatrix} \quad (3)$$

where (PIP_x, PIP_y) , (DIP_x, DIP_y) , and (Tip_x, Tip_y) are the coordinates of the points used to calculate the segment vectors of \mathbf{I}_{MCP} , \mathbf{I}_{PIP} , and \mathbf{I}_{DIP} as shown in Figure 3.2. The finger's joint angles were calculated as shown in Equations (4) and (5) for θ_{MCP} , where the rest of angles were calculated in the same manner.

$$\cos(\theta_{MCP}) = \frac{\mathbf{I}_{MCP} \cdot \mathbf{I}_{PIP}}{(\|\mathbf{I}_{MCP}\|)(\|\mathbf{I}_{PIP}\|)} \quad (4)$$

$$\theta_{MCP} = \pm 2 \tan^{-1} \left(\sqrt{\frac{1 - \cos(\theta_{MCP})}{1 + \cos(\theta_{MCP})}} \right) \quad (5)$$

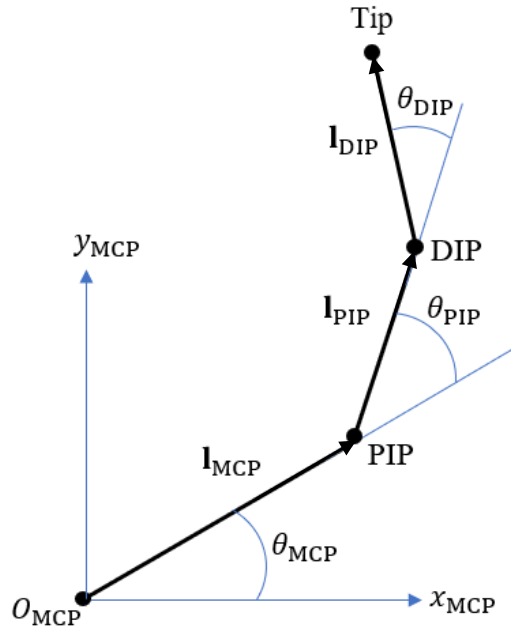


Figure 3.2 Kinematic diagram of the finger.

Figure 3.3 shows a diagram of the Denavit-Hartenberg (DH) frames attached to the actuating mechanism in its “zero-angle position,” where the mechanism consists of a prismatic and a rotary joint. The diagram is used to compare the movement of the fingertip with the movement of the actuation mechanism. The forward kinematics of the mechanism were evaluated using Equations (6) and (7).

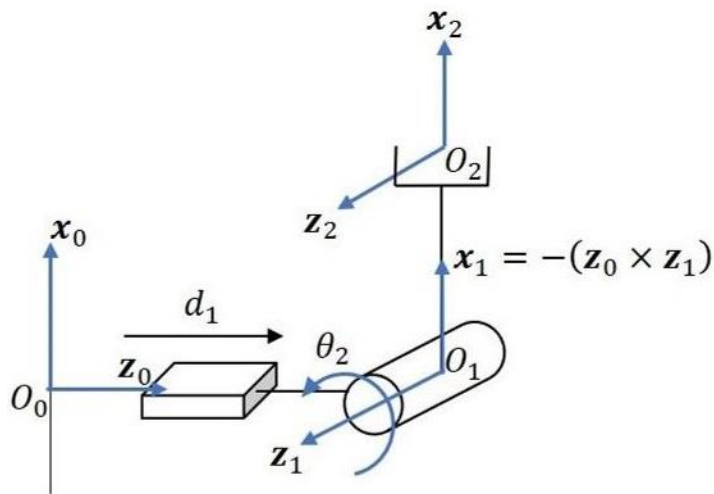


Figure 3.3 A diagram of the DH frames attached to the actuation mechanism in a zero-angle position.

$${}^0\mathbf{d}_{01} = \begin{bmatrix} 0 \\ 0 \\ d_1^* \end{bmatrix} \quad {}^1\mathbf{d}_{12} = \begin{bmatrix} 90 \cos(\theta_2^*) \\ 90 \sin(\theta_2^*) \\ 0 \end{bmatrix} \quad (6)$$

$${}^0\mathbf{d}_{02} = {}^0\mathbf{d}_{01} + {}^0\mathbf{R}_1 {}^1\mathbf{d}_{12} = \begin{bmatrix} 90 \cos(\theta_2^*) \\ 0 \\ d_1^* - 90 \sin(\theta_2^*) \end{bmatrix} \quad (7)$$

In Equation (7), ${}^0\mathbf{d}_{02}$ represents a vector from O_0 to O_2 expressed in frame $\{0\}$, which is the position of the shim's end-point connection to the finger. ${}^0\mathbf{R}_1$ represents the rotation matrix from frame $\{1\}$ to frame $\{0\}$. It should be noted that the values of DH parameters in the following table have already been used in Equations (6) and (7).

Table 3.1 DH parameters. Lengths are in mm; angles are in radians (* indicates a variable)

i	a_i	d_i	α_i	θ_i
1	0	d_1^*	$-\pi/2$	0
2	90	0	0	θ_2^*

Analysis of variance (ANOVA) was performed to investigate the effect of mass, steel thickness, and actuator type on the tip height of the model finger and the actuator velocity. The finger's tip height represents the ability of the actuating system to generate sufficient forces for lifting the suspended weights. If the actuating system is not capable of generating enough force, the tip height would remain close to its initial position. The actuator velocity demonstrates its ability to grasp and release an object in a timely manner.

3.2 Assessment of the Assembled Glove

3.2.1 Assembled Glove Motion Capture

The movement of the index finger was captured as the glove articulated it around different sized cylinders and also without the glove. The two instances were compared to see if there was any difference in the range of motion. The joint angles were also compared between the different cases. Theoretically, the differences in both the range of motion and the joint angles would decrease as the size of the cylinder increases.

3.2.2 Assembled Glove Grasping and Lifting Tests

To test how much the glove can grasp and lift in relation to the size of the object while the hand is passive, a 3D-printed container with different sized covers was used. The sizes of the cylinders were chosen by looking for common household objects that could be held with one hand. The widest objects found were 80mm in diameter and included a jar of pasta sauce, a water bottle, and a Bluetooth speaker. The narrowest object was a broom at about 30mm in diameter, but after some preliminary tests, it was determined the glove could not pick up something so thin. The second-narrowest objects found were a tube of lotion and a bottle of dish detergent, both about 40mm wide. From this search for household objects, the sizes of the cylinders were between 40mm and 80mm, increasing in width by 10mm.



Figure 3.4 Examples of common household objects. (a) a jar of pasta sauce, a water bottle, and a speaker. (b) a tube of lotion.



Figure 3.5 The container used for testing (far right) and the different caps. From left to right, the cap diameters are 40mm, 50mm, 60mm, 70mm, and 80mm. The container is also 80mm in diameter.

The most common object papers that covered grasping experiments used was a water bottle filled with 500mL of water, or weighing 500g [39], [43]. Narrow objects were either not tested or their weights were not disclosed. Water bottles are typically between 60mm and 80mm in diameter. The target of this experiment was for the glove to grasp and lift at least 500g for the 70mm and 80mm cylinders.

The experiment proceeded as follows. The container would be filled with gradually increasing weights, starting at empty and increasing in 100g increments. The user would grasp and lift the container by the cap and hold it up for five seconds. Weight would stop being added when the user is no longer able to lift the container. This was repeated for each container cap.

3.2.3 Assembled Glove Force Generation Test

To test the force generation capability of the glove, an FSR was placed on an 80mm diameter cylinder. The user was made to grasp the cylinder while having the digits applying force on the FSR one at a time for 5 seconds. This experiment was repeated five times. The data was collected with an Arduino Mega and an Adafruit data shield that is separate from the ones used in the glove's control system.

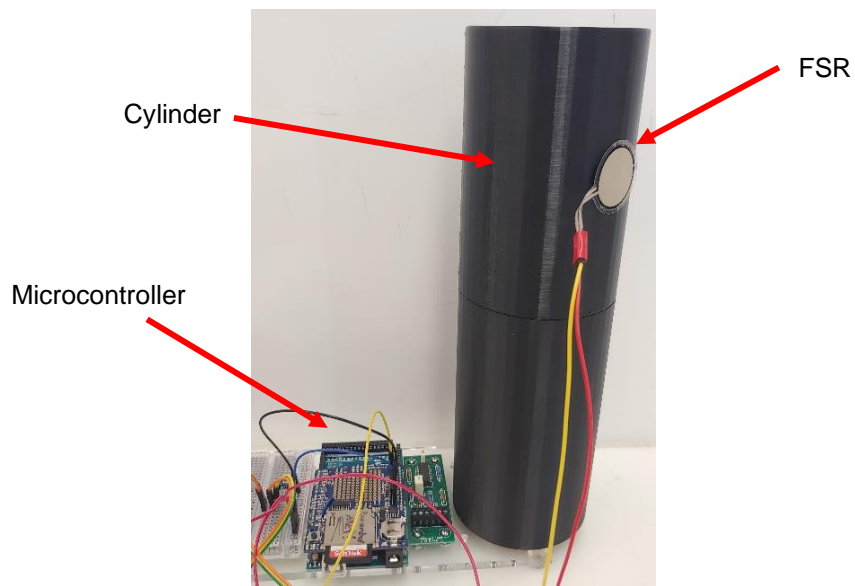


Figure 3.6 The force testing setup with the FSR attached to the side of the cylinder. The microcontroller is on the bottom left.

Force sensors must be calibrated in order to for the microcontroller to read the force value. This is done by placing objects of increasing mass on them and collecting the corresponding output signal, which is a typical process for calibrating these sensors. These points are plotted in MATLAB and a curve fitting function is used to calculate the equation that relates the output signal of the sensor with the applied force. Figure 3.7 shows the calibration curve of the FSR in Figure 3.6. The blue dots are the averages of the collected data points and the bars on each point is the standard deviation.

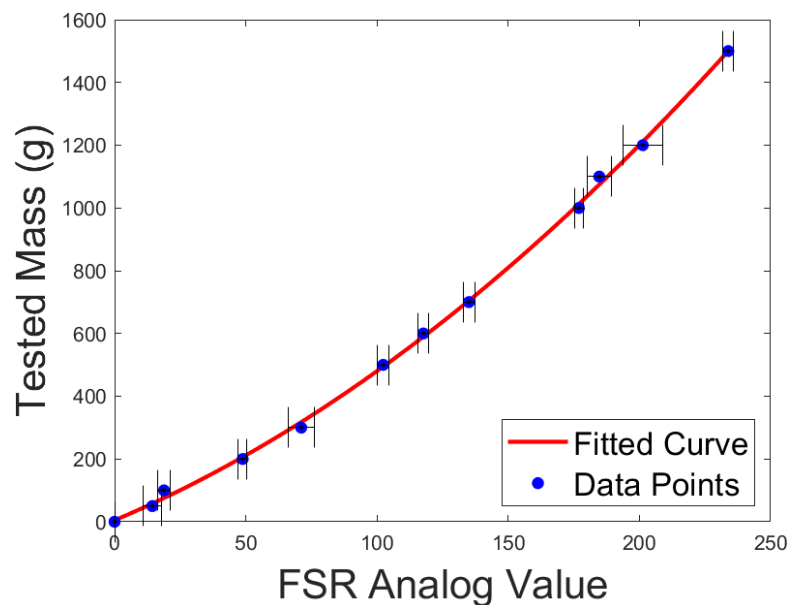


Figure 3.7 Calibration curve for the FSR used in the experiment.

Equation (8) is the equation of the fitted curve and was included in the code to convert the analog signal of the FSR to force in Newtons.

$$F = [(0.01226 \times Analog^2) + (3.527 \times Analog) + 4.815] \times 9.81/1000 \quad (8)$$

3.2.4 Assembled Glove Muscle Activity Test

To determine how effective the glove is in grasping and lifting objects while the hand is fully passive, the activity of muscles in the forearm was measured. A number of papers have measured muscle activity in their glove feasibility proofs [44], [45], [46]. Each paper focused on different muscles in their experiments. One paper measured 15 extensor and flexor muscles associated with finger movement [44]. Another measured

10 muscles [45]. One paper focused on all forearm muscle signals and machine learning to find the five signals, each one associated with a finger [46].

For the experiment for this glove, three muscles were measured, the extensor carpi radialis longus (ECRL), the flexor carpi radialis (FCR), and the flexor digitorum superficialis (FDS). Not only were these muscles measured in the previous papers, but the manufacturer for the EMG system that was used also recommended these muscles to be measured when analyzing hand grasp [47].

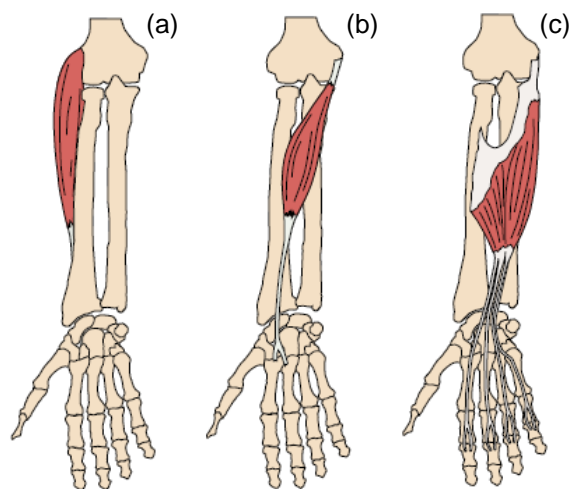


Figure 3.8 The muscles used in the experiments.
(a) ECRL, (b) FCR, and (c) FDS [47].

In reality, the EMG system does not record the activity of single muscles, but a combination of them. The only way to measure activity of individual muscles would be to insert EMGs directly into them. The ECRL and FCR actually control wrist movement but are located over muscles that do control finger movement. This means that EMGs placed on these muscles would also detect activity from the finger movement muscles that are located deeper in the arm.

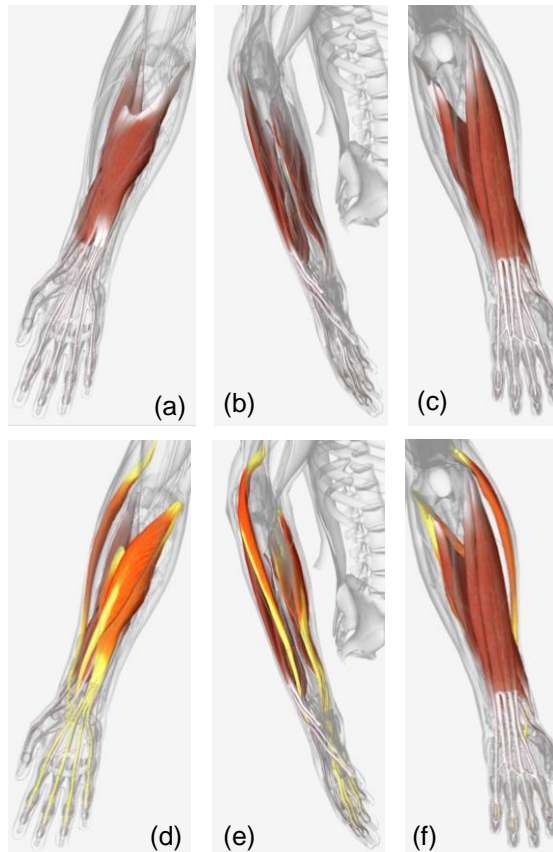


Figure 3.9 Anterior (a,d), lateral (b,e), and posterior (c,f) views of extensor and flexor muscles. (a)-(c) show the finger extensor and flexor muscles overlapping over each other and (d)-(f) show the muscles that the EMGs were positioned over [35].

This experiment consisted of two parts. The first part involved the subject grasping and raising a weighted 70mm diameter cylinder for five seconds and lower and release it for five seconds. This would be repeated five times. The second part would be the same as the first part, except the subjects would wear the glove and keep their hand passive during the experiment. The weight in the cylinder would be the maximum weight each subject could lift in the full grasp test. These last two tests would be compared to see if there is any change in muscle activity while the glove was being used.

Typically, EMG signals need to be filtered to properly analyze and view the muscle activity. This is done by calculating the root-mean-square (RMS) of the raw signal and then applying a filter to it. RMS is first used because the average of the raw

signal is always zero. RMS calculates the absolute value of the raw signal, ensuring that the data is always greater than zero, and makes the average change depending on the intensity of the muscle activity, as discussed in Chapter 10 of Winter [48]. The filter usually used is some order of a Butterworth filter with a cutoff frequency between 5Hz and 15Hz [27], [44]. Figure 3.10 shows the raw EMG signal, shown in blue, the RMS signal, shown in gray, and the filtered RMS signal, shown in red, of the maximum voluntary contraction (MVC), i.e. squeezing your hand as tightly as you can around an object, of the extensor carpi radialis longus muscle. In this case, a second order Butterworth filter with a cutoff frequency of 5 Hz was used. The sampling rate used while collecting the data was 1000 Hz.

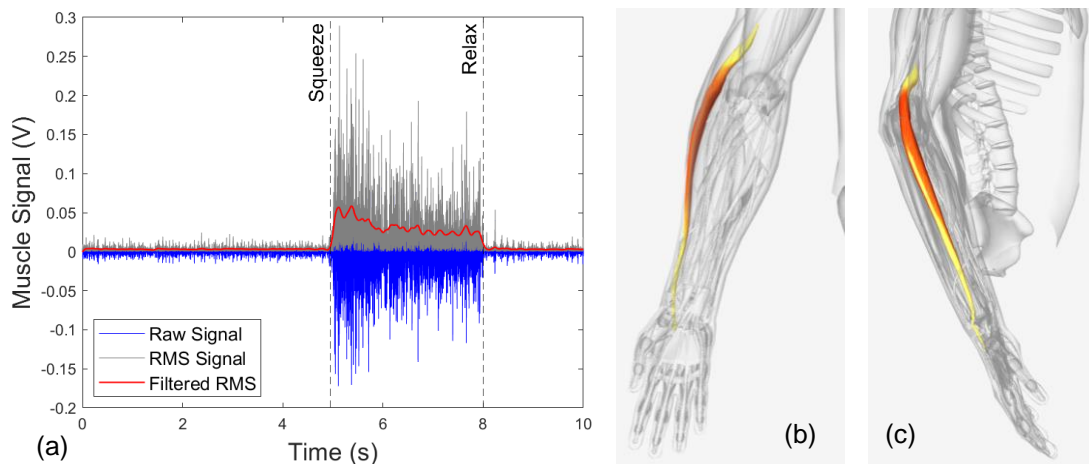


Figure 3.10 (a) The collected MVC signal of the extensor carpi radialis longus. (b) shows the muscle from the anterior side and (c) shows it from the lateral side [48].

The EMG signals was collected through Vicon Nexus software. The resting muscle signal was subtracted from the periods of activity, and the resulting signals were integrated, as discussed in Chapter 10 of Winter [48]. The difference between the integrated signals were compared between the two sets of the experiment. The following figure shows the already filtered EMG signal before the resting signal was subtracted and after. The shaded areas during the periods of activity are what were integrated.

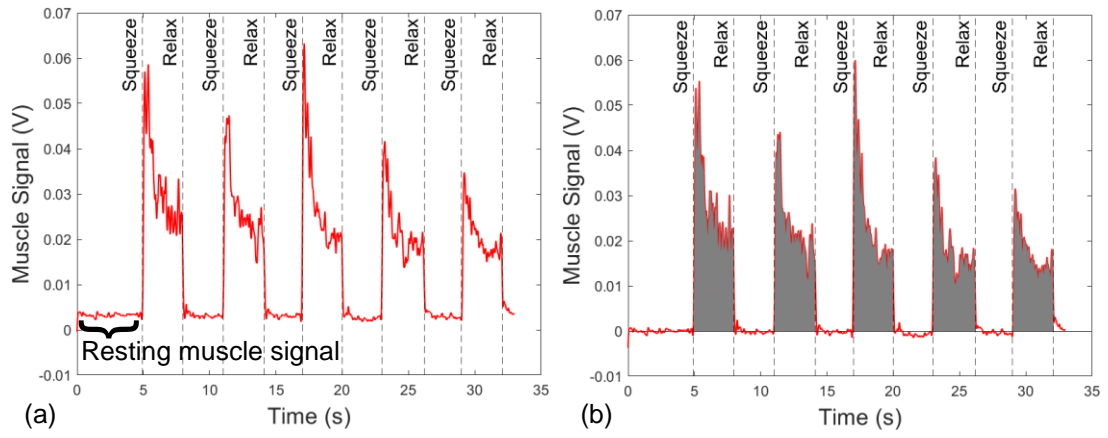


Figure 3.11 Plot of filtered muscle signal (a) before resting signal was subtracted, and (b) after. The shaded areas are what were integrated.

CHAPTER 4

RESULTS

This chapter discusses the obtained results. The feasibility of the proposed actuation mechanism is discussed first. Next, the feasibility of the glove comprised of the proposed actuation mechanism was evaluated. Force generation capability, range of motion, and the users' muscle activities are presented in detail.

4.1 Actuation Mechanism Feasibility Results

The motion data of the finger was collected using Tracker Video Analysis software and analyzed in MATLAB. Referencing the DH parameters in Table 3.1, Figure 3.3, and Equations (6) and (7), the coordinates of ${}^0\mathbf{d}_{02}$ are expressed in the axes of frame {0} and are shown by the blue circles in Figure 4.1. The red crosses in Figure 4.1 show the position of the fingertip expressed in the axes of frame {MCP} relative to its origin O_{MCP} .

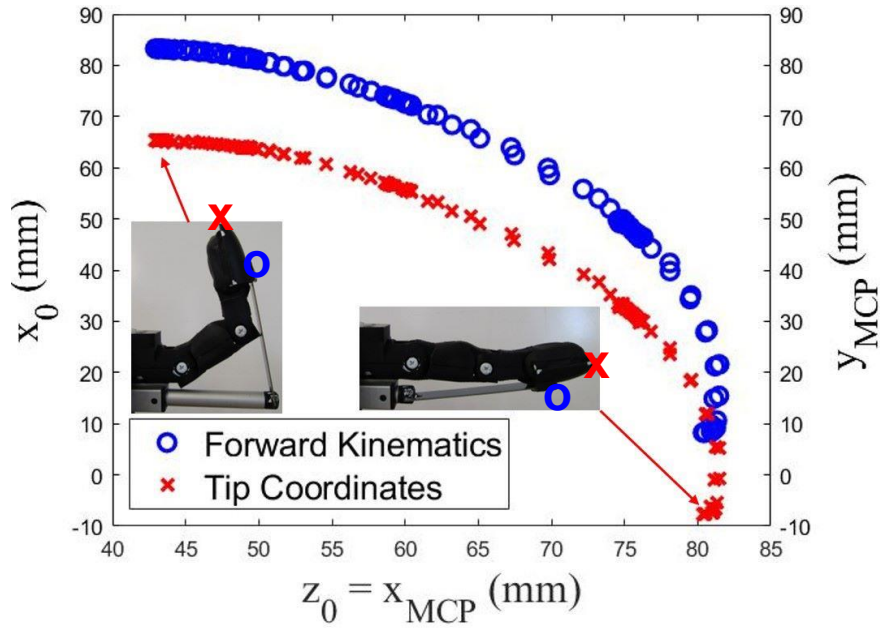


Figure 4.1 Graphical representation of the workspace of the actuation mechanism (blue “o”) and the fingertip coordinates (red “x”). The left y-axis shows the shim’s height from the forward kinematics analysis, while the right y-axis shows the height of the fingertip from motion capture analysis.

In Figure 4.1, the left y-axis shows the shim’s position obtained from forward kinematics analysis relative to O_0 and along the x_0 -axis, whereas the right y-axis shows the fingertip’s position relative to O_{MCP} along y_{MCP} -axis. It should be noted that for frames $\{0\}$ and $\{MCP\}$, the x_{MCP} -axis equals to the z_0 -axis. The difference between the two sets of points in Figure 3.4 is due to there being a physical offset between the origin of the linear actuator’s coordinate system O_0 and the MCP joint center O_{MCP} . These results show the capability of the actuating system in properly bending the finger for grasping an object.

A relation between the stroke length d_1 and the ${}^0\mathbf{d}_{02}$ coordinate along x_0 can be properly approximated by a second-order polynomial with an R^2 value of 0.996. This establishes a direct relationship between the stroke length and the position of the finger and its bending curvature, given that θ_2 cannot be directly measured. This can be used to estimate the position of the fingertip given the stroke length of the linear actuator.

4.1.1 Steel Thickness

Analyzing the finger's profiles for both actuators and strips showed that the profiles adversely changed with increasing the mass when using the 0.010" spring steel (i.e., the thinner one). Comparing the tip height versus the actuator's stroke length, it was observed that the finger did not move uniformly due to the high load. Figure 4.2 shows the height (i.e., the coordinate along y_{MCP} -axis from the initial position) of the PIP and DIP joints and the fingertip versus the stroke length. The dashed vertical lines indicate the stroke increments of 12.5mm, 25mm, 37.5mm, and 50mm.

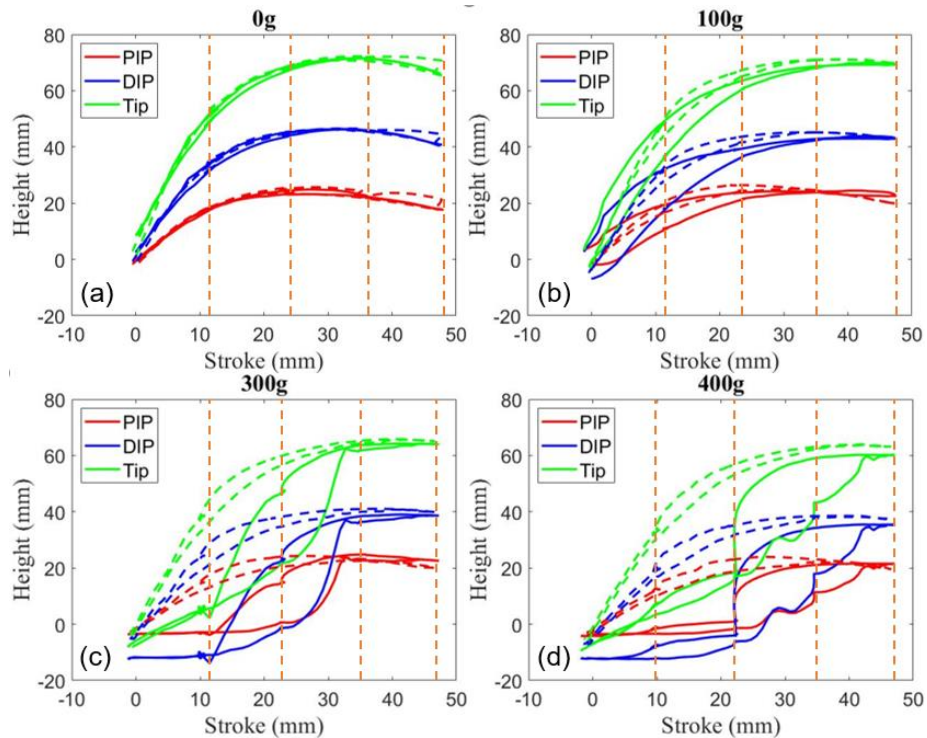


Figure 4.2 Finger joints' heights when using the L12 actuator with (a) no load, (b) 100g, (c) 300g, and (d) 400g. Solid lines represent the 0.010" strip while the dashed lines represent the 0.025" strip. The vertical dashed lines indicate the stroke increments. The profiles for different masses using the L16 actuator follow similar patterns.

The solid lines are the profiles when the 0.010" steel strip was tested, and the dashed lines are the profiles when the 0.025" strip (i.e., the thicker strip) was tested. As one can see, the profiles for both strips at 0g are nearly identical. As the mass increased, the changes became more pronounced in the thinner strip while the profiles for the thicker

one remained consistent during increasing the mass. The finger's behavior for the thinner strip was due to the fact that as the actuator extended farther and the mass increased, the strip bent more extremely. The thinner strip would eventually straighten and force the finger up rapidly like a released spring, which can be seen in the solid green line in Figures 4.2(c) and (d). In addition, the calculated stiffnesses of the strips in Subsection 2.2 (27.32N/m for the 0.01" strip and 427.35N/m for the 0.025" strip) indicated that the thinner strip may not be able to lift the finger as effectively as the thicker one, thus making it the lower limit of the range discussed in Subsection 2.2. This and the results from Figure 4.2 indicate that the thin strip is not sufficient for transmitting the force.

The unnatural movement of the finger with the thinner strip at heavier masses such as 300g and 400g yielded unnatural joint angles as well, especially in the DIP joint. As shown in Figure 4.3, the behavior of the model finger using the thin strip 0.010" deviates from what would be expected of a real finger, in which the DIP angle is typically less than the PIP angle in an index and middle finger [49].

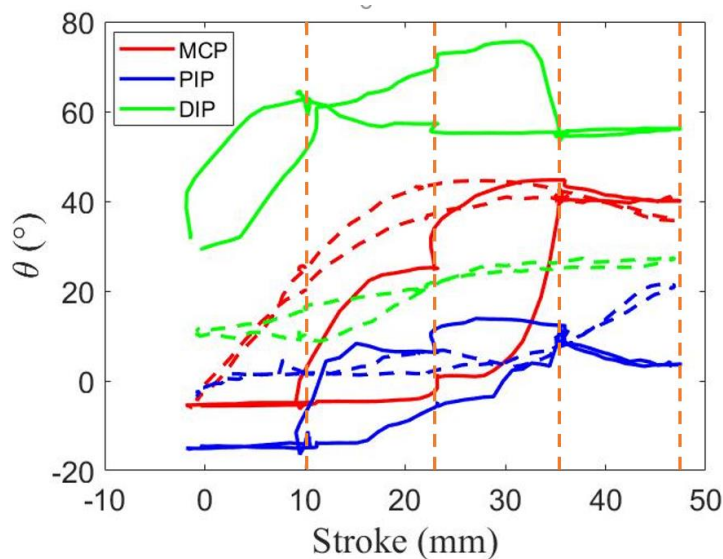


Figure 4.3 Joint angles of the model finger under the L12 actuator, 0.010" strip, while lifting a 300g mass. Solid lines represent the 0.010" strip and dashed lines represent the 0.025" strip. The vertical dashed lines indicate the stroke increments. Similar behavior was observed when using the L16 actuator, or when using heavier masses.

A 2-way ANOVA analysis was also performed to compare the effects of mass and steel thickness on the height of the fingertip when the actuator was fully extended. Each spring steel was tested in 50 experimental trials (i.e., 2 actuators x 5 weight conditions x 5 repetitions). It was observed that strip thickness and mass parameters both significantly (with $\alpha = 0.05$) affected the fingertip height at the full extension of the actuator. As Figure 4.4 demonstrates, the thicker strip increased the tip height significantly under a load ($p < 0.001$) and generated greater forces over the range of tested masses compared to the thinner strip. It was found that increasing the mass significantly reduced the tip height ($p < 0.001$).

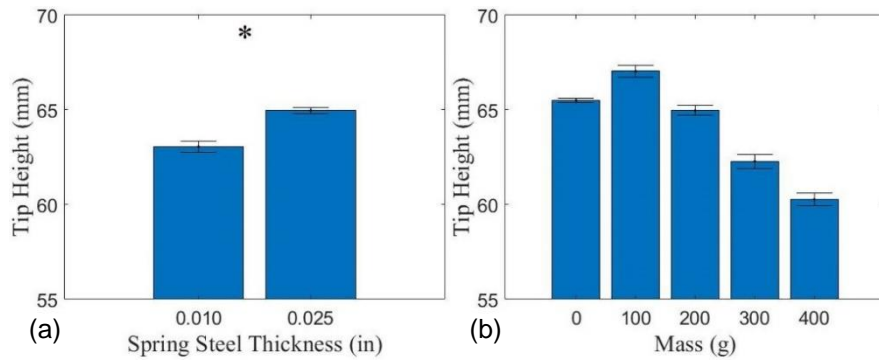


Figure 4.4 Bar plots show the means and standard errors of the fingertip height at the actuators' full extension for different (a) strip thicknesses and (b) masses (* indicates a significant difference between the conditions).

4.1.2 Actuator Type

Another design parameter investigated in this study was the effect of linear actuator type (i.e., L12 and L16) on the performance of the actuating system. As a performance indicator, the velocity of the actuator extension and retraction was examined under different actuator types and mass conditions. As mentioned earlier, the velocity quantifies the responsiveness of the actuating system when assisting the user during grasping and releasing of an object. The tip height was not considered in this analysis due to a slight height difference between the two actuators' mounting setup and its effect on the tip height measurements. However, it was demonstrated that both

actuators could achieve adequate tip height under various mass conditions as presented in Subsection 4.1.1. Figure 4.5 shows the full extension and retraction velocities of the actuators for different masses and strip thicknesses.

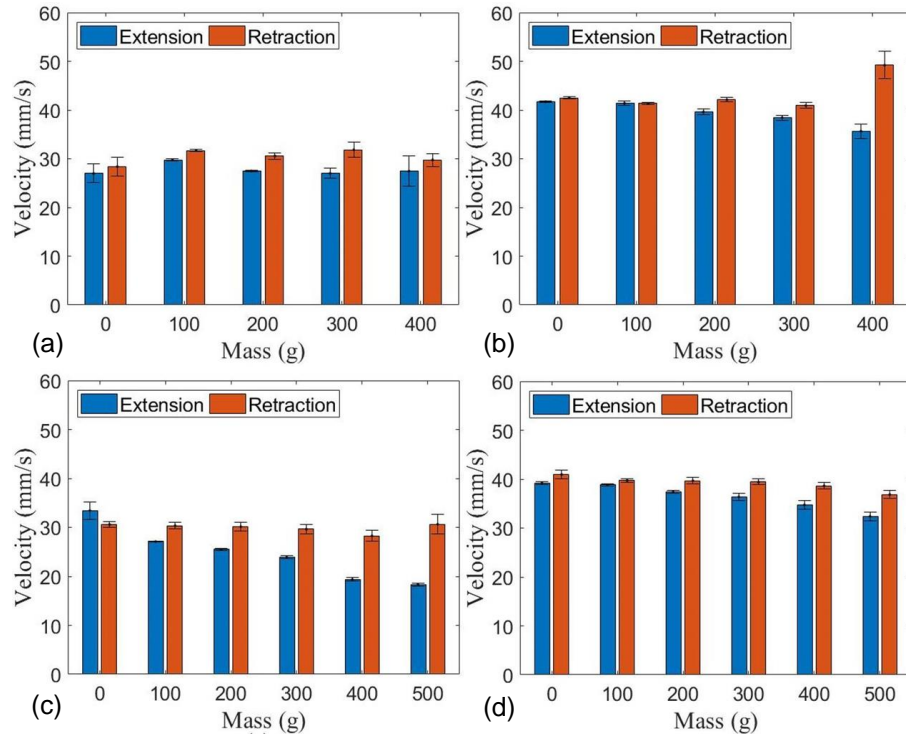


Figure 4.5 Bar plots show the means and standard errors of the extension and retraction velocities of both actuators and strips tested by different masses. The (a) L12 actuator with 0.010" strip, (b) L16 actuator with 0.010" strip, (c) L12 actuator with 0.025" strip, and (d) L16 actuator with 0.025" strip.

Almost in all cases, the retraction velocity was faster than the extension one due to the effect of gravity. It was also found that the actuator type significantly affected the velocity of the actuating system. The L16 results in faster extension and retraction under a load than the L12 due to its lower gear ratio. There were no significant differences in the retraction velocities across the range of tested masses. The 0.010" strip yielded faster extension velocities for the L12 actuator than the 0.025" strip, most likely because of the extreme bending of the 0.010" strip and its rapid release similar to a spring as mentioned earlier, which can be seen in Figure 4.5. Comparing the actuators when 0.025" strip was tested, the increase of mass had a more pronounced effect on the

extension velocity of the L12 (shown in Figure 4.5(c)) than the extension velocity of the L16 (shown in Figure 4.5(d)). At the extreme case of a 500g mass, the L16 actuator could extend 77% faster than the L12.

Using a 2-way ANOVA to further investigate the effects of mass and actuator type on the extension and retraction velocities, it was found that both of these variables were statistically significant with $p < 0.001$, as depicted in Figure 4.6. Only the actuator type was a significant variable affecting the retraction velocity $p < 0.001$, whereas the effect of mass on the retraction velocity was not significant ($p = 0.659$).

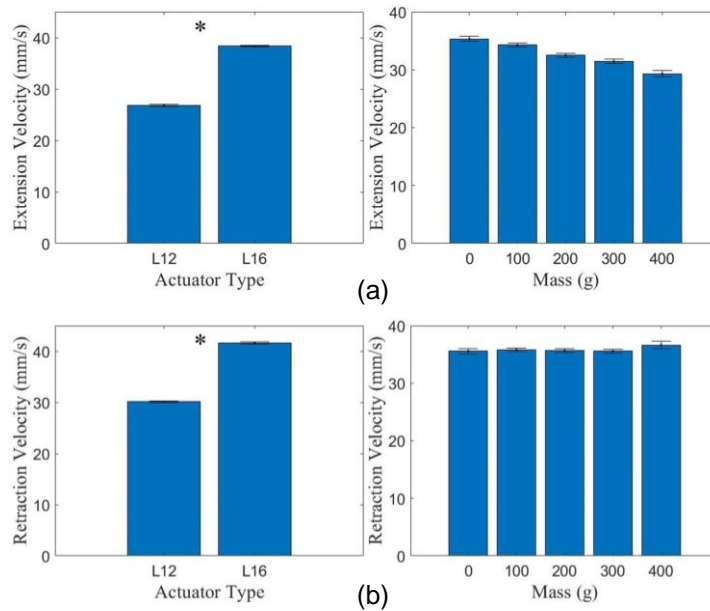


Figure 4.6 Bar plots show the means and standard errors of the extension velocities. (a) Extension velocity and (b) retraction velocity for different actuator types and masses. The * indicates a significant difference between the conditions.

4.1.3 Other Effects

Figure 4.7 shows the average tip height at each stroke increment versus the mass. The actuators and spring steels had similar trends when lifting the weights. As the mass increased, the tip height decreased. As the stroke increased, the tip height increased, but the thickness of the steel affected how much the finger rose at each stroke increment. Shown in Figure 4.7(b), the tip heights for a 400g mass at 1/4, 1/2,

and 3/4 of the L16 full stroke when using the 0.010” strip are much lower than the tip heights for the 0.025” strip as shown in Figure 4.7(d). The same comparison can be made between Figures 4.7(a) and (c) when the L12 was used. Table 4.1 summarizes the comparisons between the effects of different masses on the extension and retraction velocities and the tip heights.

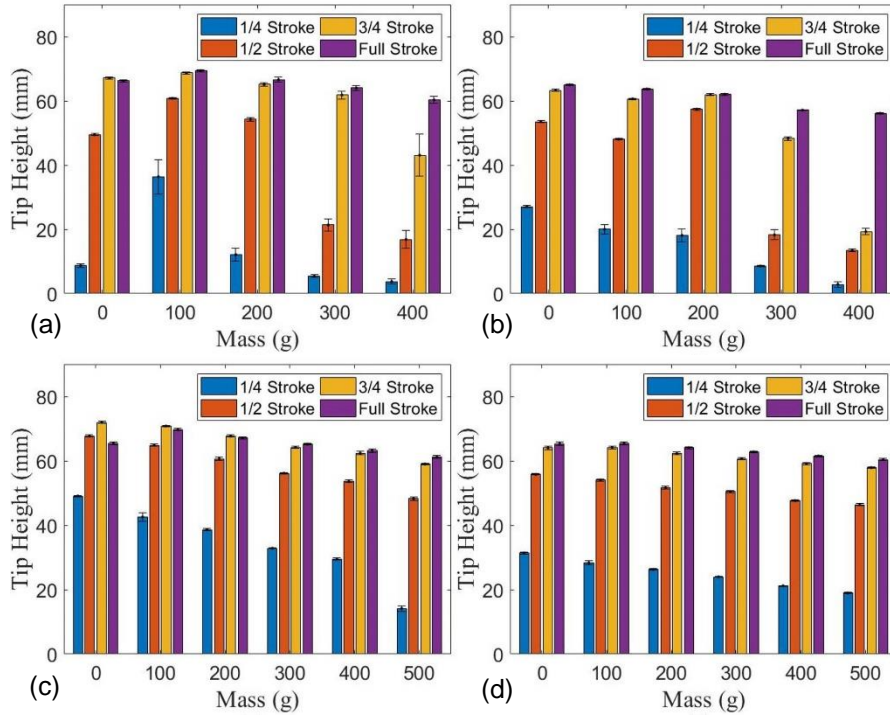


Figure 4.7 Bar plots show the mean and standard errors of the tip height for both actuators and strips tested by different masses. The (a) L12 actuator with 0.010” strip, (b) L16 actuator with 0.010” strip, (c) L12 actuator with 0.025” strip, and (d) L16 actuator with 0.025” strip.

Table 4.1 Pairwise comparison of different masses affecting the dependent variables (* indicates a significant difference between pairs)

Mass Comparison		Extension Velocity <i>p</i> -value	Retraction Velocity <i>p</i> -value	Tip Height <i>p</i> -value
0g	100g	0.673	0.998	0.223
0g	200g	0.003*	1.000	0.948
0g	300g	< 0.001*	1.000	< 0.001*
0g	400g	< 0.001*	0.700	< 0.001*
100g	200g	0.169	1.000	0.042*
100g	300g	0.003*	0.997	< 0.001*
100g	400g	< 0.001*	0.863	< 0.001*
200g	300g	0.666	1.000	0.004*
200g	400g	0.001*	0.761	< 0.001*
300g	400g	0.058	0.675	0.053

The time of extension and retraction can be also calculated from the velocities and the stroke lengths. On average, it took about 1.3 seconds for the L16 to extend and another 1.2 seconds for it to retract. These times makes the design suitable for rehabilitation exercises, in which repetitive extensions/flexions need to be performed. It has been reported that an average of about two seconds per cycle would be sufficient for rehabilitation purposes and performing ADL [27]. The actuating system's response time is within a reasonable range of this reported value.

4.2 Assistive Glove Design

The assistive glove was constructed with two L16 actuators with a 50mm stroke fixed on a 3D-printed base located on the dorsal side of a glove and an L12 actuator with a 30mm stroke fixed on another 3D-printed base on the dorsal side of the thumb's MCP joint as shown in Figure 4.8.

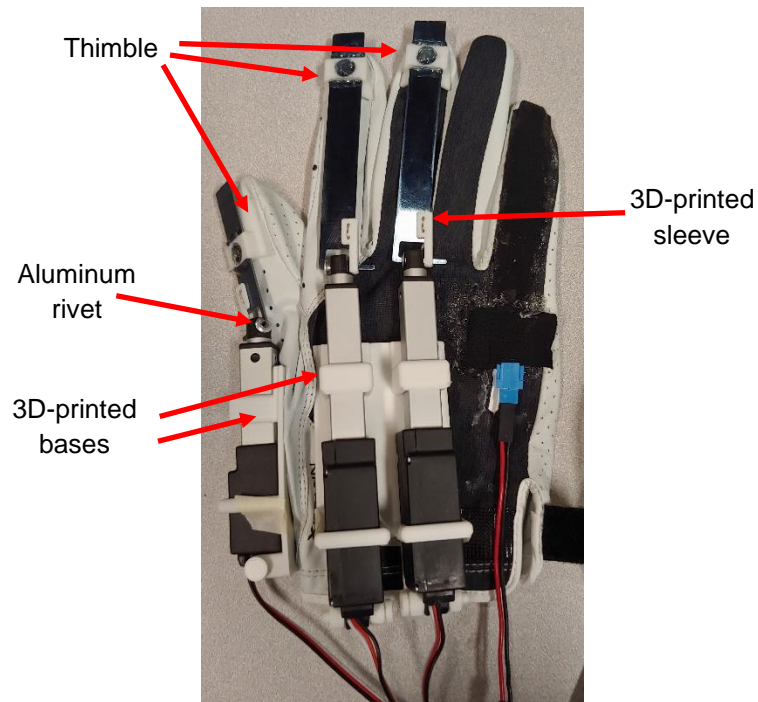


Figure 4.8 The assembled assistive glove.

The spring steel is attached to the actuator with a small aluminum rivet that allows the user to still move his or her fingers side to side in addition to flexing and extending them during the glove's operation. The steel strips are held in place with a small 3D-printed sleeve. Two holes in the sleeve line up with holes in the strip to insert a small piece of wire to fix the sleeve in place. The thimble that connects the steel strip to the finger has a slot so it could be properly adjusted for the user's finger lengths. The glove is a men's golf glove. This was chosen for its good grip and tight fit on the hand. All the components of the actuation mechanisms attached to the glove make the glove lightweight at 196g, easy to don and remove, and customizable. In addition, the glove itself may be changed depending on the hand size of the user. Currently, there are three sizes available for users to choose from: medium, large, and extra-large. These are shown in Figure 4.9.

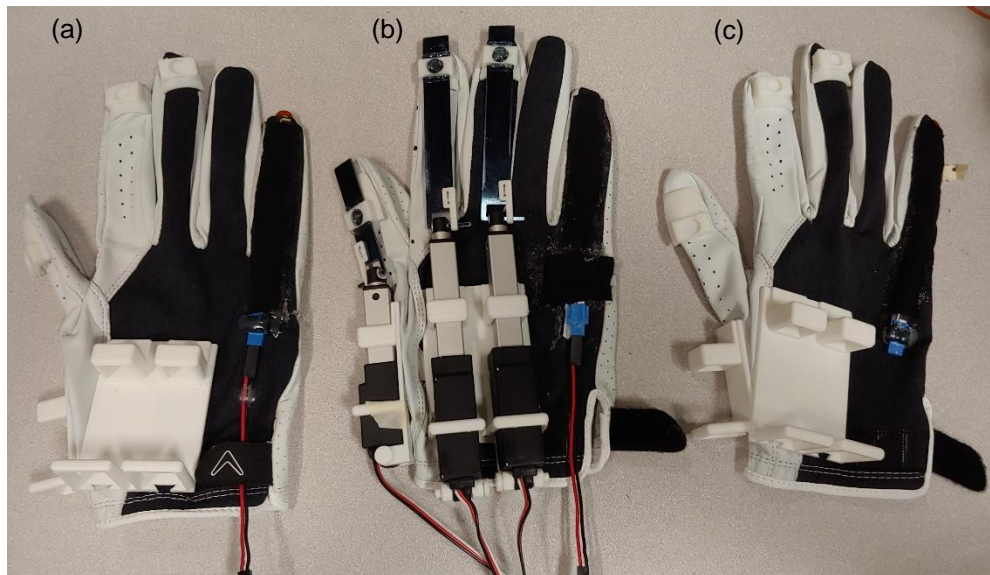


Figure 4.9 The three different gloves available for users. (a) medium, (b) large, and (c) extra-large. The large glove has the actuating mechanism connected to it.

The control system consists of an Arduino Mega and an Adafruit Data Shield. It is powered with a 3.7V 2500mAh LiPo battery and an Adafruit PowerBoost 1000c. The PowerBoost converts the 3.7V into 5V at 1A current that may be used to power the control system. This is all housed in a 3D-printed box that may be mounted on the

forearm. The control system and housing weigh 208g, slightly heavier than the actuation mechanism on the glove. CAD design iterations of the thimbles, actuator bases, and control system housing can be found in the Appendix. Additionally, design iterations of the spring steel can be found there.

The new power source could allow the actuators to fully extend in 1.1 seconds and retract in 1.2 seconds and give the glove a maximum run time of 2.5 hours. A larger battery may be used for longer use time. The actuators may be controlled with either a flex sensor that is attached to the pinky finger or a separate two-button control box. The flex sensor option works such that when users flexes their pinky finger, the actuators fully extend. When the pinky finger is extended, the actuators fully retract. The control box option works by pressing the “OUT” button to fully extend the actuators and pressing the “IN” button to fully retract them. Figure 4.10 shows the control system inside its housing, the battery connected to the PowerBoost, and the two control options for the glove.

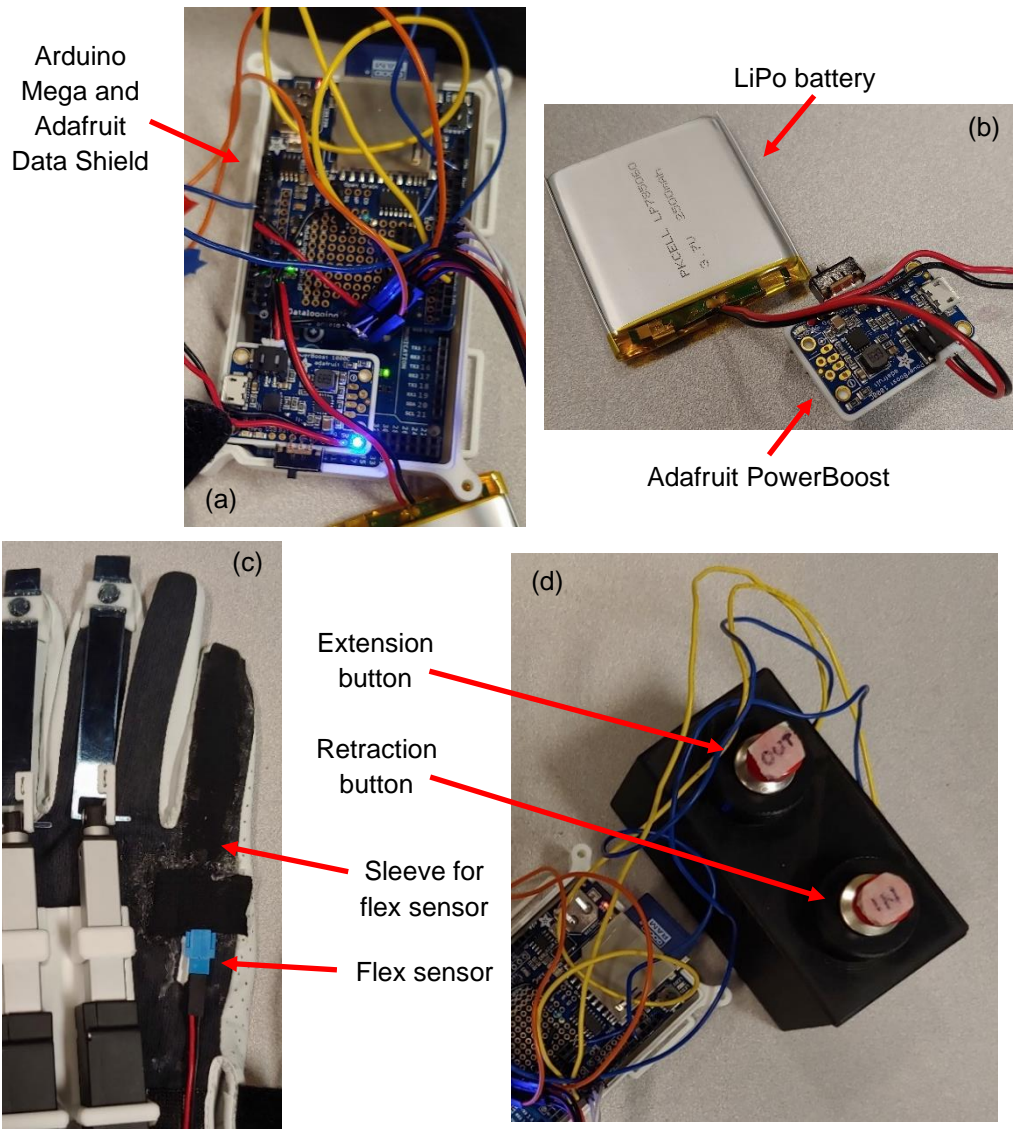


Figure 4.10 (a) The control system hardware inside the housing and (b) the battery connected to the PowerBoost. (c) and (d) show the two different control mechanisms: a flex sensor inside a sleeve on the pinky finger and a control box.

As previously mentioned, the part of the assistive glove worn on the hand (i.e., the actuators, spring steels, and the glove) weighs 196g and the control system hardware in its housing weighs 208g, making the entire device weigh 404g. The weight of the glove is close to others already developed, such as the one by In, et al. [10] at 194g and the one by Nycz, et al. [36] at 113g. The weight of the control system in its housing is much lighter than Nycz's, which weighed 754g, but was heavier than the assistive glove developed by Popov, et al. [1], which weight 90g. Figure 4.11 shows the

glove being worn with the control system worn on the forearm. The flex sensor option is implemented in this image.

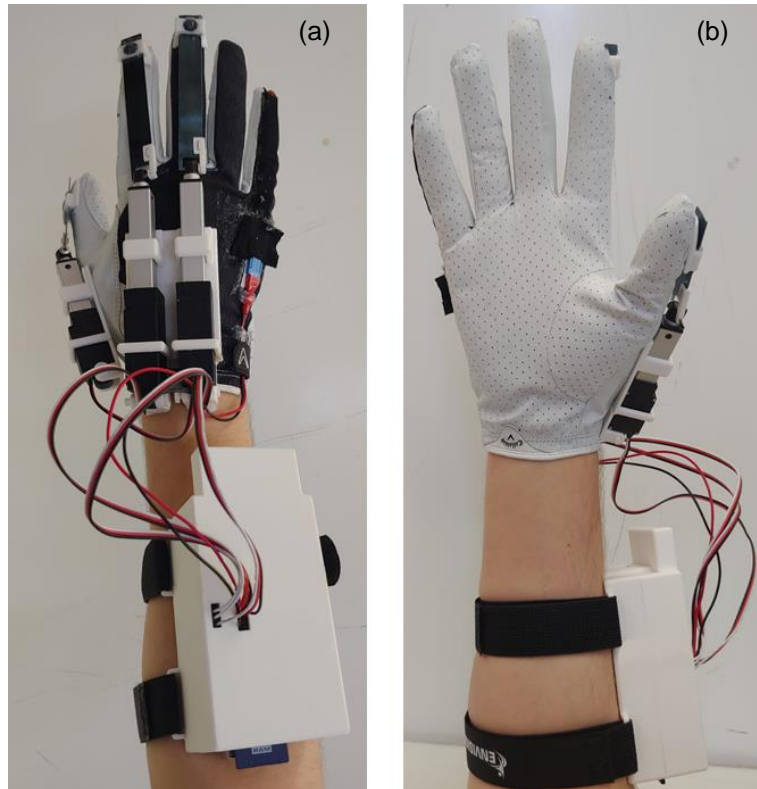


Figure 4.11 The fully assembled glove worn on the right hand with the pinky finger flex sensor control option implemented. (a) anterior view and (b) posterior view.

The assistive glove costs about \$311 to make. A breakdown of the cost of the glove can be found in Table 4.2. The majority of the cost came from the three linear actuators which totaled \$210. The remainder of the cost went towards electronics, 3D printed parts, and the physical glove. Adhesives and wires were not included in the cost rundown.

Table 4.2 Cost breakdown of the assistive glove. (~ indicates an estimated cost as it depends on where the parts are printed)

Part	Amount	Price
3.7V 2500mAh LiPo battery	1	\$14.95
3D-printed mounts and housings (FDM)	11	~\$5.00
3D-printed thimbles (SLA)	3	~\$5.20
Adafruit Data Shield	1	\$13.95
Adafruit PowerBoost 1000C	1	\$19.95
Callaway men's golf glove	1	\$19.95
Flex sensor	1	\$10.74
Generic Arduino Mega	1	\$10.99
L12 30mm stroke actuator	1	\$70.00
L16 50mm stroke actuator	2	\$140.00
Total		\$310.73

4.3 Assessment of the Glove's Performance

To evaluate the performance of the glove, its force generation, range of motion, and muscle activity reduction of the user were investigated using six young male adults. The purpose of these pilot tests was to inform the function and capabilities of the glove for future studies. An IRB was submitted and under review based on the results discussed in this section in order to do further testing that would focus on human performance.

4.3.1 Glove Assembly

The experiments started off with each subject having their right index finger measured for proper motion capture. Next, the subject donned a disposable nitrile glove before trying on the assistive glove to keep it clean. As mentioned before, three sizes of the assistive glove were available for the subjects to try on. Once the appropriate glove was selected by the subject, the actuation mechanism was attached. The actuators were put in place first, followed by the steel strips. The strips were fixed into place in the thimbles with a hot glue gun, as shown in Figure 4.12.



Figure 4.12 The steel strip for the thumb being fixed to the thimble.

4.3.2 Assembled Glove Motion Capture Results

The first experiment conducted was motion capture of the index finger. Each subject had the free movement of their right index finger video recorded with a camera. The glove was then donned, and the subjects used the glove to wrap their hands around the different sized cylinders. The motion of the index finger was captured during each trial. The final motion capture contained the free movement of the index finger actuated by the glove. These videos were then uploaded to the Tracker software to be analyzed. Figure 4.13 are screenshots of motion capture analysis in progress.

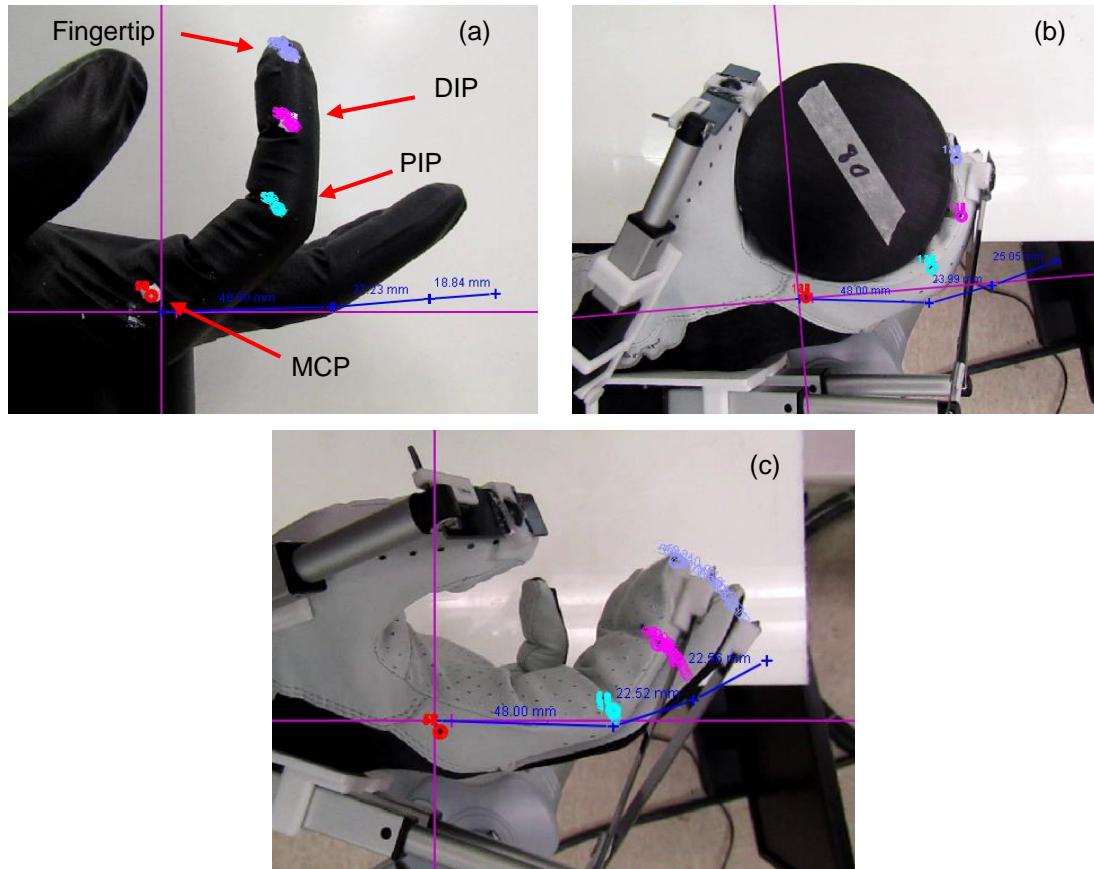


Figure 4.13 Screenshots of the Tracker software for (a) a free-moving finger, (b) a cylinder, and (c) a finger freely actuated by the glove.

Data from all six subjects were collected. From this point on, the subjects will be referred to as A, B, C, D, E, and F. The finger lengths of each subject and glove sizes the subjects chose is found in Table 4.3.

Table 4.3 Index finger lengths of each subject and their respective glove sizes

Subject	Finger Length (mm)	Glove Size
A	89	M
B	102	L
C	95	XL
D	97	L
E	85	M
F	101	L

The workspace of the index finger was analyzed for three cases: when it was curling around a 40mm cylinder, 80mm cylinder, and when it was grasping nothing.

Figure 4.14 shows the workspaces of each case from each subject.

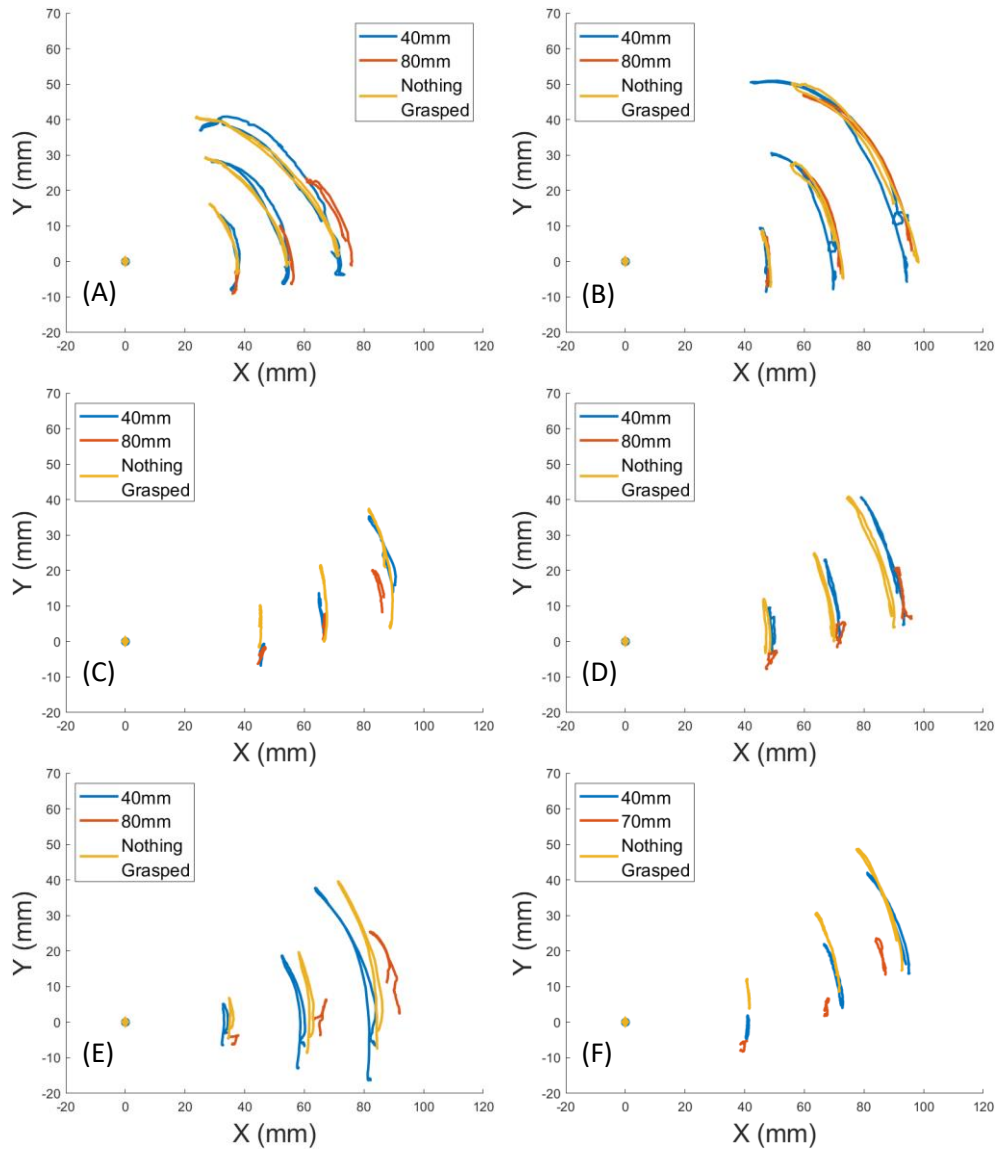


Figure 4.14 Finger joint motion profiles of each subject while grasping a 40mm cylinder, 80mm cylinder, and nothing. The final plot (F) has the motion profile of Subject F grasping a 70mm cylinder instead because that was the largest object he could grasp.

The workspace of the finger decreases as the size of the cylinder increases, as was expected. The workspace when the subjects grasp the 40mm cylinder is very similar to the empty grasp, but thanks to the thumb's actuation, they are still able to grasp and manipulate the small cylinder. Figure 4.15 shows a comparison of the finger movement profiles from one subject when he grasps a 40mm cylinder and 80mm cylinder, as well as the free movement of the index finger.

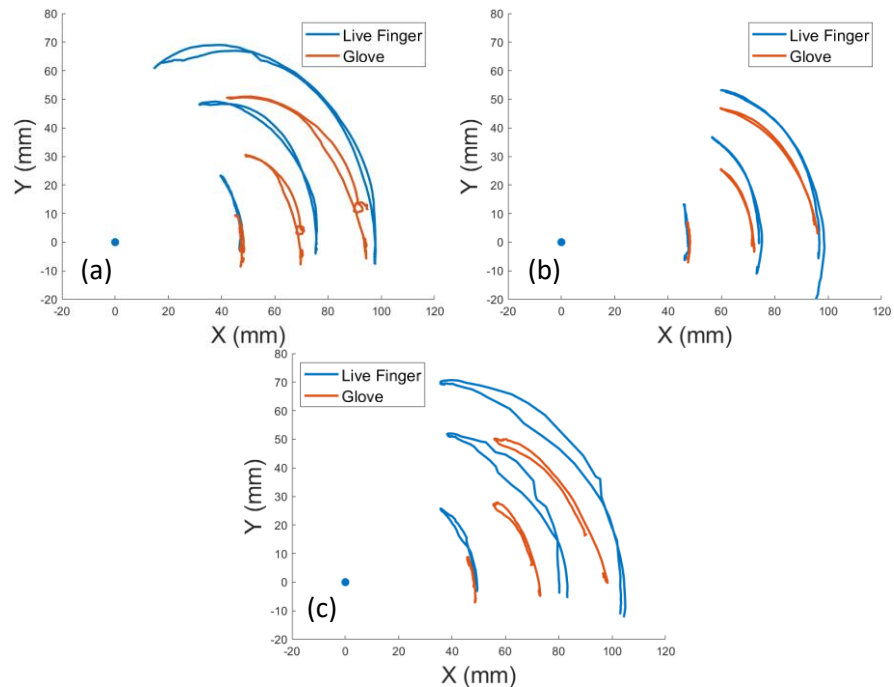


Figure 4.15 The finger joint motion profiles of (a) a 40mm cylinder, (b) an 80mm cylinder, and (c) free movement when Subject B is wearing the glove and when he isn't. The point in the lower left-hand part of each plot is the stationary MCP joint and the rightmost profiles are those of the fingertip.

The live finger profiles in Figure 4.15(a) and (c) are much greater than the profiles of the gloved finger. The profiles of the two cases in Figure 4.15(b) are very similar, most likely due to the size of the object. Despite the gloved finger profile not fully lining up with the live finger profile, the glove still adequately actuates the fingers for the hand to successfully grasp and manipulate each object.

The final part of the motion capture analysis was to calculate the joint angles of the index finger for the live finger and the gloved finger at maximum flexion using Equations (1) – (5) in Chapter 3. Figure 4.16 shows the average angles of each joint from all of the subjects for each case. The PIP joint has greatest angle for the live finger case and gloved finger case, 62.6° and 35.2° , respectively. For the live finger case, the MCP has the second-highest angle at 38.7° and the DIP last at 26.6° . For the gloved finger case, the MCP has the lowest angle at 15.8° , and the DIP is slightly higher at 17.8° . These angles are tabulated in Table 4.4.

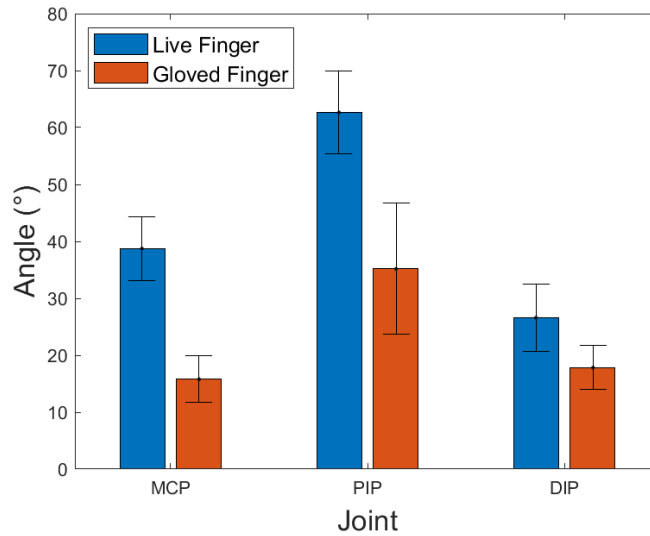


Figure 4.16 Joint angles of the index finger when the glove is not used (blue) and when it is used (red).

Table 4.4 The average angles of the live index finger and gloved index finger at maximum flexion along with their respective standard deviations.

	MCP		PIP		DIP	
	Average	Standard Deviation	Average	Standard Deviation	Average	Standard Deviation
Live Finger	38.7°	11.3°	62.6°	14.6°	26.6°	11.8°
Gloved Finger	15.8°	8.2°	35.2°	23.0°	17.8°	7.7°

4.3.3 Assembled Glove Grasping and Lifting Results

The goal of the next experiment was to see how much weight the subjects could lift with the glove while the hand was passive in relation to the size of the object. The subjects started at no added load (0g) for each cylinder and had the weight increased by 100g until they could no longer maintain a grasp on the cylinder. The experiment is shown being conducted with a 70mm cylinder and 40mm cylinder in Figure 4.17.

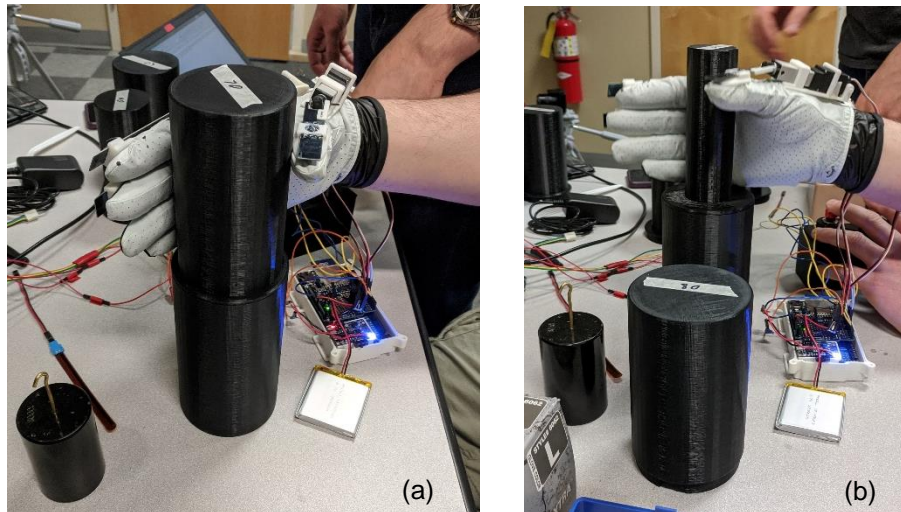


Figure 4.17 The experiment being conducted with a subject attempting to grasp (a) a 70mm cylinder and (b) a 40mm cylinder.

Data from Subjects B, C, E, and F were used in the full grasp test. Figure 4.18 shows the average weight that could be lifted by the users in relation to the size of the cylinder. The maximum average liftable weights were 350g, 600g, 975g, 1025g, and 1000g, from smallest diameter to largest. As mentioned in Subsection 3.2.2, the goal was for the glove to lift at least 500g with the 60mm, 70mm, and 80mm cylinders. This experiment showed that it was more than capable of doing this. The data also shows that as the size of the cylinder increased, the more weight the subject could lift. This was most likely due to there being more surface contact with between the larger cylinders and the glove.

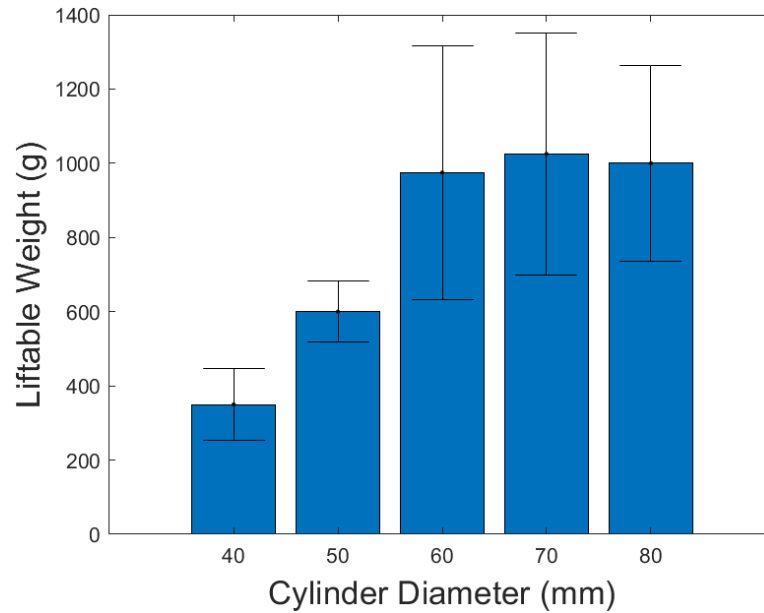


Figure 4.18 Liftable weight in relation to the size of the cylinder.

4.3.4 Assembled Glove Force Generation Results

Force generation by the glove was collected using a force-sensitive resistor (FSR) connected to an Arduino Mega and Adafruit data shield. This microcontroller setup was separate from the one being used to control the glove. The microcontroller was coded to take the analog input of the FSR and convert it to force in Newtons using Equation (8).

The data shield, shown in Figure 3.6, had an SD card which collected the force data that was then transferred to the computer for analysis. The FSR was attached to the largest cylinder the subject could grasp, and force data was captured by each finger individually. Figure 4.19 shows the setup in use by a subject with the microcontroller collecting force data from the middle finger.

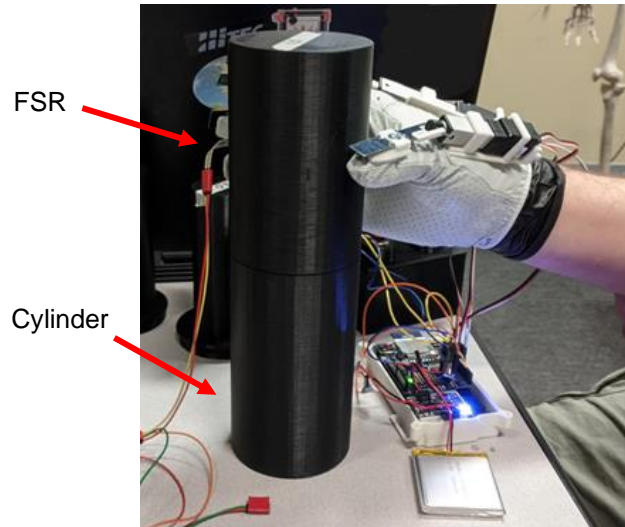


Figure 4.19 A subject grasping the 80mm cylinder with the FSR collecting force data from the middle finger.

Force data was collected from all six subjects. Figure 4.20 shows the average force generated by the glove on each digit when the users grasped the widest cylinder they could with the glove.

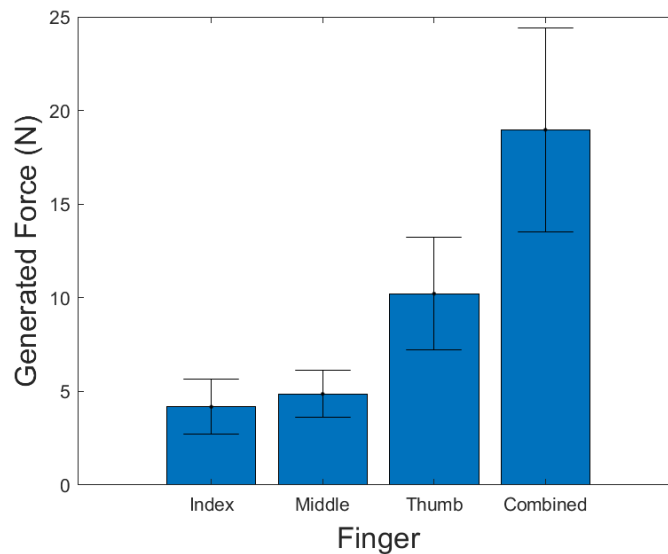


Figure 4.20 Force generated by each digit on the cylinder.

As previously stated in Chapter 2, the acceptable range of force generation for each finger is 3N-5N [1], [18], [20]. The glove is able to generate force within that range for the index and middle fingers (an average of 4.2N and 4.9N, respectively). The thumb can apply an average of 10.2N of force with the glove, well beyond the target range.

This makes the total average force generated with the glove to be 19.3N, showing that the glove can provide adequate force generation to manipulate objects in ADL [1], [18], [20].

4.3.5 Assembled Glove Muscle Activity Analysis

Muscle activity data from the extensor carpi radialis longus (ECRL), flexor carpi radialis (FCR), and flexor digitorum superficialis (FDS) was recorded from four subjects. Two cases were tested. The first case was when the subjects manipulated a weighted 70mm cylinder without the glove and the second case was when they manipulated the cylinder with the glove. Figure 4.21 shows a subject performing the experiment while wearing the glove.

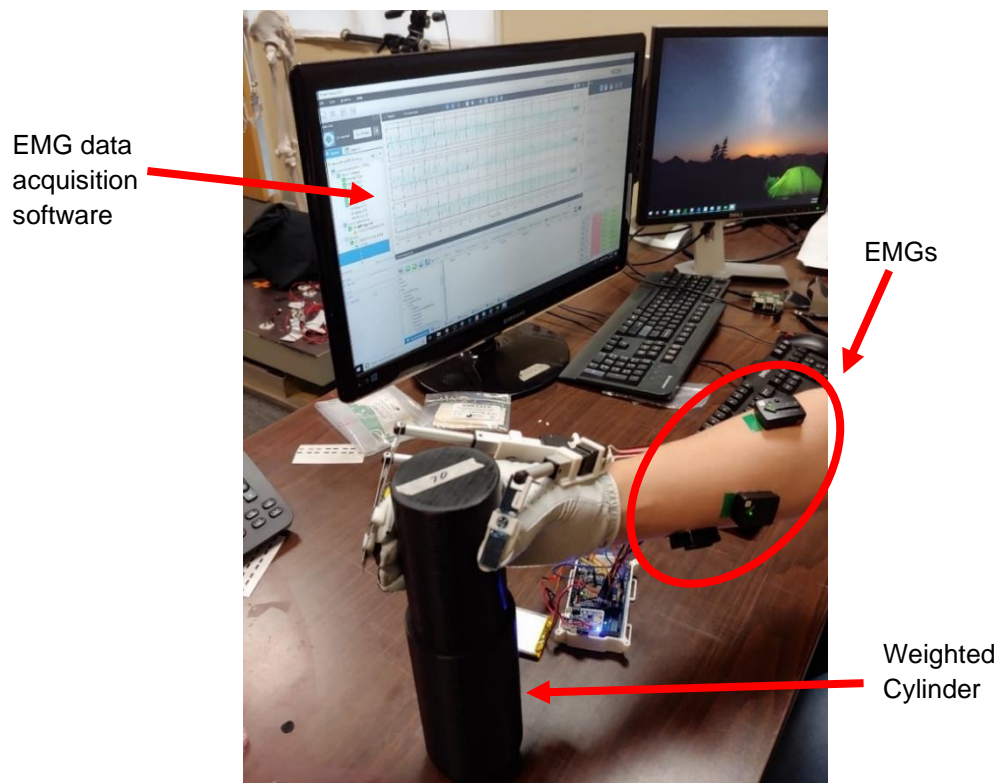


Figure 4.21 The EMG reading being acquired while the subject gets ready to lift the cylinder.

The following plots in Figure 4.22 show the observed muscle activity of the FDS when the glove was not used and when it was used.

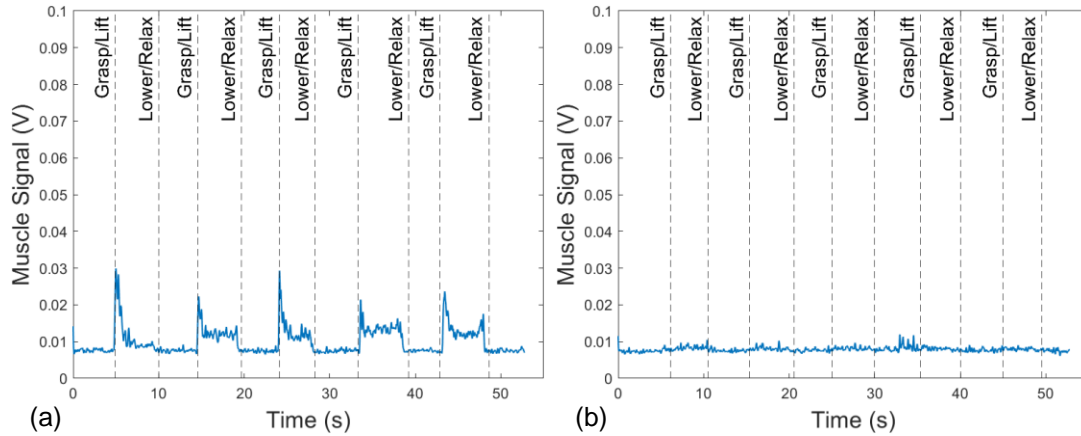


Figure 4.22 Muscle activity of the FDS of Subject B (a) when the glove was not used and the hand was active, and (b) when the glove was used and the hand was passive.

Figure 4.23 shows the average of the muscle activity while the hand was manipulating the cylinder during the two cases and the percent decrease in muscle activity between the case of lifting an object without the glove and with the glove.

Activity decreases 21% in the ECRL, 80.8% in the FCR, and 76.1% in the FDS.

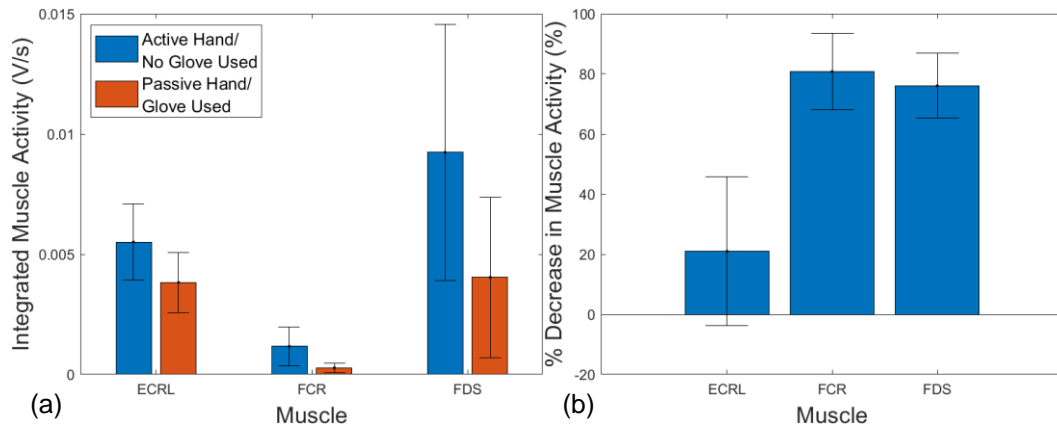


Figure 4.23 (a) Average muscle activity while the cylinder was manipulated. (b) Percent decrease in muscle activity between the case of lifting an object with and without the glove.

A t-test was also conducted to further compare the muscle activity between the two cases. Both tests were conducted 20 times (i.e., 4 subjects x 5 repetitions) to determine the p -values of the three muscles between the two experiments. It was observed that the glove significantly affected the subjects' abilities to grasp the cylinder, with the p -values for all of the muscles being less than 0.01, which can be seen in Table 4.5 along with the average percent differences and standard deviations. These results

further prove that with the hand being completely passive, the glove is still able to lift heavy objects. Since the glove is intended for people who just need extra help, not those who have completely lost their grasping abilities, it should not have any difficulty assisting with ADL.

Table 4.5 Average percent differences, standard deviations, and pairwise comparison of glove affecting the muscle activity (* indicates a significant difference between pairs)

	Average Percent Difference	Standard Deviation	p-value
ECRL	21.0	49.5	< 0.001*
FCR	80.8	25.4	0.0051
FDS	76.1	21.5	< 0.001*

CHAPTER 5

CONCLUSION

The purpose of this thesis was to design an assistive glove for people who need additional help with activities of daily living (ADL). This includes grasping and holding household objects like a filled water bottle, cans of food, or a tube of lotion. A significant amount of work went into researching current designs of gloves to see how they worked and what could be learned from them. A design for the actuation mechanism consisting of a strip of spring steel attached at one end to a linear actuator and the fingertip at the other end was devised, and vigorous testing was conducted on it to determine its feasibility. Once it was proven that the proposed design would work, the rest of the glove was designed.

The proposed glove was intended to actuate the index finger, middle finger, and thumb. This was successfully done using two actuation mechanisms with L16 actuators for the fingers and one mechanism with an L12 actuator for the thumb. The control system was constructed using an Arduino Mega, an Adafruit Data Shield, and a flex sensor attached to the pinky finger of the glove. The entire system was powered with a 3.7V 2500mAh LiPo battery giving the glove a maximum run time of 2.5 hours. The goal was to have the glove and control system weigh less than 500g. The resulting weight was 400g.

The glove was intended to grasp and lift objects between 60mm and 80mm in diameter weighing at least 500g while the subject's hand was completely passive. Experiments showed that it was capable of lifting around double this target. The

next goal for the glove was for it to generate 3N-5N in each digit. The glove succeeded in generating forces within this range for the index and middle fingers and around 10N for the thumb.

The final experiment was to see if having the glove grasp and lift a heavy object while the subject's hand was passive resulted in a noticeable decrease in muscle activity. Three muscles were tested using EMGs: the extensor carpi radialis longus, the flexor carpi radialis, and the flexor digitorum superficialis. The results from this experiment showed that muscle activity decreased 21% in the ECRL and around 80% in the two flexor muscles. Statistical analysis further proved that the use of the glove significantly affected the muscle activity and allowed users to grasp objects greater than 500g without the use of their own strength.

All in all, the glove exceeded expectations. The target demographic of the glove was people with only diminished grasping abilities. However, all of the tests were conducted while the hand was fully passive. From this analysis, it was shown that the glove helps in assisting with ADL and can grant those with diminished hand grasping abilities greater independence.

5.1 Possibilities for Future Investigation

A number of things may be improved to the design and testing of the assistive glove. Most importantly, more human testing must be done to show stronger evidence that the glove does what has been claimed. A group of healthy adults over the age of 55 should be brought in for testing, since age is a factor in decreased hand grasping abilities. Pinch gripping is an important test that many scholars have tested. Similar experiments should be done with this glove to determine its capabilities in being able to pick up and hold things like a pen, cooking utensil, or a toothbrush.

One thing that was noticed throughout the second half of the research is that the surface of the glove can affect how much of a grip a user can have on an object. The golfer's glove performed well in the test described in Subsection 4.3.3, but if the entire palmar side was coated with a material of a higher friction coefficient (i.e., silicone or rubber), the glove may be able to hold even heavier objects, especially those with smaller sizes.

REFERENCES

- [1] Dmitry Popov, Igor Gaponov, and Jee-Hwan Ryu, Portable Exoskeleton Glove with Soft Structure for Hand Assistance in Activities of Daily Living, in *IEEE/ASME Trans. Mechatronics*, vol. 22, pp. 865-875, April 2017.
- [2] Pinhas Ben-Tzvi and Zhou Ma, Sensing and Force-Feedback Exoskeleton (SAFE) Robotic Glove, in *IEEE Trans. Neural Syst. Rehabil. Eng.*, vol. 23, pp. 992-1002, November 2015.
- [3] Heidi C. Fischer, et al., Use of a Portable Assistive Glove to Facilitate Rehabilitation in Stroke Survivors with Severe Hand Impairment, in *IEEE Trans. Neural Syst. Rehabil. Eng.*, vol. 24, pp. 344-351, March 2016.
- [4] Zhou Ma and Pinhas Ben-Tzvi, Design and Optimization of a Five-Finger Haptic Glove Mechanism, in *ASME J. Mechanisms and Robot.*, vol. 7, November 2015.
- [5] Sangwoo Park, Lauri Bishop, Tara Post, Yuchen Xiao, Joel Stein, and Matei Ciocarlie, On the Feasibility of Wearable Exotendon Networks for Whole-Hand Movement Patterns in Stroke Patients, in *Proc. IEEE Int. Conf. on Robot. Autom. (ICRA)*, Stockholm, 2016, pp. 3729-3735.
- [6] Hong Kai Yap, Phone May Khin, Tze Hui Koh, Yi Sun, Xinquan Liang, Jeong Hoon Lim, and Chen-Hua Yeow. A Fully Fabric-Based Bidirectional Soft Robotic Glove for Assistance and Rehabilitation of Hand Impaired Patients, in *IEEE Robot. Autom. Letters*, vol. 2, pp. 1383– 1390, July 2017.
- [7] Brian Byunghyun Kang, Haemin Lee, Hyunki In, Useok Jeong, Jinwon Chung, and Kyu-Jin Cho, Development of a Polymer-Based Tendon-Driven Wearable Robotic Hand, in *Proc. IEEE Int. Conf. on Robot. Autom. (ICRA)*, Stockholm, 2016, pp. 3750-3755.
- [8] Benjamin W. Gasser, Daniel A. Bennett, Christina M. Durrrough, and Michael Goldfarb, Design and Preliminary Assessment of Vanderbilt Hand Exoskeleton, in *Proc. IEEE Int. Conf. Rehab. Robot. (ICORR)*, London, 2017, pp. 1537-1542.
- [9] Michael A. Delph II, Sarah A. Fischer, Phillip W. Gauthier, Carlos H. Martinez Luna, Edward A. Clancy, and Gregory S. Fischer, A Soft Robotic Exomusculature Glove with Integrated sEMG Sensing for Hand Rehabilitation, in *Proc. IEEE Int. Conf. Rehab. Robot. (ICORR)*, Seattle, 2013, pp. 1-7.
- [10] Hyunki In, Brian Byunghyun Kang, MinKi Sin, and Kyu-Jin Cho, Exo-Glove: A Wearable Robot for the Hand with a Soft Tendon Routing System, in *IEEE Robot. Autom. Mag.*, vol. 22, pp. 97-105, March 2015.

- [11] Christopher J. Nycz, Michael A. Delph, and Gregory S. Fischer, Modeling and Design of a Tendon Actuated Soft Robotic Exoskeleton for Hemiparetic Upper Limb Rehabilitation, in Proc. 2015 37th Annu. Int. Conf. of the IEEE Eng. in Med. and Bio. Soci. (EMBC), Milan, 2015, pp. 3889-3892.
- [12] Stuart Biggar and Wei Yao, Design and Evaluation of a Soft and Wearable Robotic Glove for Hand Rehabilitation, IEEE Trans. Neural Syst. Rehabil. Eng., vol. 24, pp. 1071-1080, October 2016.
- [13] Lei Cui, Anthony Phan, and Garry Allison, Design and Fabrication of a Three Dimensional Printable Non-Assembly Articulated Hand Exoskeleton for Rehabilitation, in 2015 37th Annu. Int. Conf. of the IEEE Eng. in Med. and Bio. Soci. (EMBC), Milan, 2015, pp. 4627-4630.
- [14] N.S.K. Ho, K.Y. Tong, X.L. Hu, K.L. Fung, X.J. Wei, W. Rong, E.A. Susanto, An EMG-driven Exoskeleton Hand Robotic Training Device on Chronic Stroke Subjects, in Proc. IEEE Int. Conf. Rehab. Robot. (ICORR), Zurich, 2011, pp. 1-5.
- [15] Jumpei Arata, Keiichi Ohmoto, Roger Gassert, Olivier Lambercy, Hideo Fujimoto, and Ikuo Wada, A new hand exoskeleton device for rehabilitation using a three-layered sliding spring mechanism, in Proc. IEEE Int. Conf. on Robot. Autom. (ICRA), Karlsruhe, 2013, pp. 3902-3907.
- [16] Duojin Wang, Qingyun Meng, Qiaoling Meng, Xinwei Li, and Hongliu Yu, Design and Development of a Portable Exoskeleton for Hand Rehabilitation, in IEEE Trans. Neural Syst. Rehabil. Eng., vol. 26, pp. 2376-2386, December 2018.
- [17] Yasuhisa Hasegawa, Yasuyuki Mikami, Kosuke Watanabe, and Yoshiyuki Sankai, Five-Fingered Assistive Hand with Mechanical Compliance of Human Finger, in Proc. IEEE Int. Conf. on Robot. Autom. (ICRA), Pasadena, 2008, pp. 718-724.
- [18] Pinhas Ben-Tzvi, Jerome Danoff, and Zhou Ma, The Design Evolution of a Sensing and Force-Feedback Exoskeleton Robotic Glove for Hand Rehabilitation Application, in ASME J. Mechanisms and Robot., vol. 8, October 2016.
- [19] Hong Kai Yap, Jeong Hoon Lim, Fatima Nasralla, James C.H. Goh, and Ray C.H. Yeow, A Soft Exoskeleton for Hand Assistive and Rehabilitation Application using Pneumatic Actuators with Variable Stiffness, in Proc. IEEE Int. Conf. on Robot. Autom. (ICRA), Seattle, 2015, pp. 4967-4972.
- [20] Panagiotis Polygerinos, Zheng Wang, Kevin C. Galloway, Robert J. Wood, and Conor J. Walsh, Soft robotic glove for combined assistance and at-home rehabilitation, in Robot. and Auton. Syst., vol. 73, pp. 135-143, November 2015.

- [21] Lauri Connelly, Yicheng Jia, Maria L. Toro, Mary Ellen Stoykov, Robert V. Kenyon, and Derek G. Kamper, A Pneumatic Glove and Immersive Virtual Reality Environment for Hand Rehabilitative Training After Stroke, in IEEE Trans. Neural Syst. Rehabil. Eng., vol. 18, pp. 551-559, October 2010.
- [22] Alberto Borboni, Maurizio Mor, and Rodolfo Faglia, Gloreha – Hand Robotic Rehabilitation: Design, Mechanical Model, and Experiments, in ASME J. Dyn. Syst., Meas., Control, vol. 138, November 2016.
- [23] Panagiotis Polygerinos, Kevin C. Galloway, Siddharth Sanan, Maxwell Herman, and Conor J. Walsh, EMG Controlled Soft Robotic Glove for Assistance During Activities of Daily Living, in Proc. IEEE Int. Conf. Rehab. Robot. (ICORR), Singapore, 2015, pp. 55-60.
- [24] Kotaro Tadano, Masao Akai, Kazuo Kadota, and Kenji Kawashima, Development of Grip Amplified Glove using Bi-articular Mechanism with Pneumatic Artificial Rubber Muscle, in Proc. IEEE Int. Conf. on Robot. Autom. (ICRA), Anchorage, 2010, pp. 2363-2368.
- [25] Lucas Gerez, Junan Chen, and Minas Liarokapis, On the Development of Adaptive, Tendon-Driven, Wearable Exo-Gloves for Grasping Capabilities Enhancement, in IEEE Robot. Autom. Letters, vol. 4, pp. 422-429, April 2019.
- [26] HyunKi In and Kyu-Jin Cho, Evaluation of the antagonistic tendon driven system for SNU Exo-Glove, in Proc. 2012 9th Int. Conf. on Ubiquitous Robot. and Ambient Intell. (URAI), Daejeon, 2012, pp. 507-509.
- [27] Panagiotis Polygerinos, Kevin C. Galloway, Emily Savage, Maxwell Herman, Kathleen O'Donnell, and Conor J. Walsh, Soft Robotic Glove for Hand Rehabilitation and Task Specific Training, in Proc. IEEE Int. Conf. on Robot. Autom. (ICRA), Seattle, 2015, pp. 2913-2919.
- [28] Yongkang Jiang, Diansheng Chen, Jiacheng Que, Zhe Liu, Ziqi Wang, and Ying Xu, Soft Robotic Glove for Hand Rehabilitation Based on a Novel Fabrication Method, in Proc. IEEE Int. Conf. Robot. and Biomimetics (ROBIO), Macau 2017.
- [29] "Force Sensors." Tekscan. <https://www.tekscan.com/force-sensors> (accessed Jan. 18, 2020).
- [30] "Standard Sensors." SingleTact. <https://www.singletact.com/micro-force-sensors/standard-sensors/> (accessed Jan. 18, 2020).

- [31] “Subminiature Industrial Load Cell, Metric, 0-10 to 0-10,000 Newtons.” Omega Engineering. <https://www.omega.com/en-us/sensors-and-sensing-equipment/load-and-force/load-cells/p/LCMKD> (accessed Jan. 18, 2020).
- [32] R. S. Behnke, “Movement,” in *Kinetic Anatomy*, 3rd ed., Champaign, IL, USA: Human Kinetics, Inc., 2012, ch. 2, pp. 29-35.
- [33] J. Langman and M. W. Woerdeman, “Upper Limb,” in *Atlas of Medical Anatomy*, 2nd ed. Philadelphia, PA, USA: W. B. Saunders Company, 1982, ch. 4, pp. 205-272.
- [34] W. D. Gardner and W. A. Osburn, “The Muscular System,” in *Structure of the Human Body*, 2nd ed., Philadelphia, PA, USA: W. B. Saunders Company, 1973, ch. 4, pp. 151-238.
- [35] “Upper Limb.” BioDigital. <https://human.biodigital.com/view?id=39Ut&lang=en> (accessed Jan. 18, 2020).
- [36] Christopher J. Nycz, Tobias Bützer, Olivier Lambercy, Jumpei Arata, Gregory S. Fischer, and Roger Gassert, Design and Characterization of a Lightweight and Fully Portable Remote Actuation System for Use with a Hand Exoskeleton, in *IEEE Robot. Autom. Letters*, vol. 1, pp. 976-983, July 2016.
- [37] Tobias Bützer, et al., PEXO – A Pediatric Whole Hand Exoskeleton for Grasping Assistance in Task-Oriented Training, in *Proc. 2019 IEEE Int. Conf. Rehab. Robot. (ICORR)*, Toronto, 2019, pp. 108-114.
- [38] “L12-R Micro Linear Servos for RC & Arduino.” Actuonix Motion Devices Inc. <https://www.actuonix.com/L12-R-Linear-Servo-For-Radio-Control-p/l12-r.htm> (accessed Feb. 3, 2019).
- [39] “L16-R Miniature Linear Servos for RC & Arduino.” Actuonix Motion Devices, Inc. <https://www.actuonix.com/L16-RMiniature-Linear-Servo-For-RC-p/l16-r.htm> (accessed Feb. 3, 2019).
- [40] Vinoth K. Ranganathan, Vlodek Siemionow, Vinod Sahgal, and Guang H. Yue, Effects of Aging on Hand Function, in *J. of Amer. Geriatrics Soc.*, vol. 49, pp. 1478-1484, November 2001.
- [41] Sofia Brorsson, Anna Nilsson, Carina Thorstensson, and Ann Bremander, Differences in muscle activity during hand-dexterity tasks between women with arthritis and a healthy reference group, in *BMC Musculoskeletal Disorders*, vol. 15, May 2014.
- [42] “Tracker Video Analysis and Modeling Tool for Physics Education.” Physlets. <https://www.physlets.org/tracker/> (accessed Mar. 31, 2020).

- [43] Daniel A. Bennett, Skyler A. Dalley, Don Truex, and Michael Goldfarb, A Multigrasp Hand Prosthesis for Providing Precision and Conformal Grasps, in IEEE/ASME Trans. Mechatronics, vol. 20, pp. 1697-1704, August 2015.
- [44] Sashwati Geed and Peter L. E. van Kan, Grasp-Based Functional Coupling Between Reach- and Grasp-Related Components of Forelimb Muscle Activity, in J. Motor Behav., vol. 49, pp. 312-328, September 2016.
- [45] Nadine Fligge, Holger Urbanek, Patrick van der Smagt, Relation between object properties and EMG during reaching to grasp, in J. Electromyography and Kinesiology, vol. 23, pp. 402-410, April 2013.
- [46] Arjan Gijsberts, Manfredo Atzori, Claudio Castellini, Henning Müller, and Barbara Caputo, Movement Error Rate for Evaluation of Machine Learning Methods for sEMG-Based Hand Movement and Classification, in IEEE Trans. Neural Syst. Rehabil. Eng., vol. 22, pp. 735-744, July 2014.
- [47] “Technical Note 101: EMG Sensor Placement.” Delsys.
<https://www.delsys.com/downloads/TECHNICALNOTE/101-emg-sensor-placement.pdf>
(accessed Mar. 10, 2020).
- [48] D. A. Winter, *Biomechanics and Motor Control of Human Movement*, 4th ed., Hoboken, NJ, USA: John Wiley & Sons, Inc., 2009.
- [49] Cynthia C. Norkin and D. Joyce White, “The Hand”, in *Measurement of Joint Motion: A Guide to Goniometry*, 4th ed. Philadelphia: F.A. Davis, 2009, ch. 7, pp.143-192.

APPENDIX

Figure A.1 Design iterations of the dorsal actuator mount.

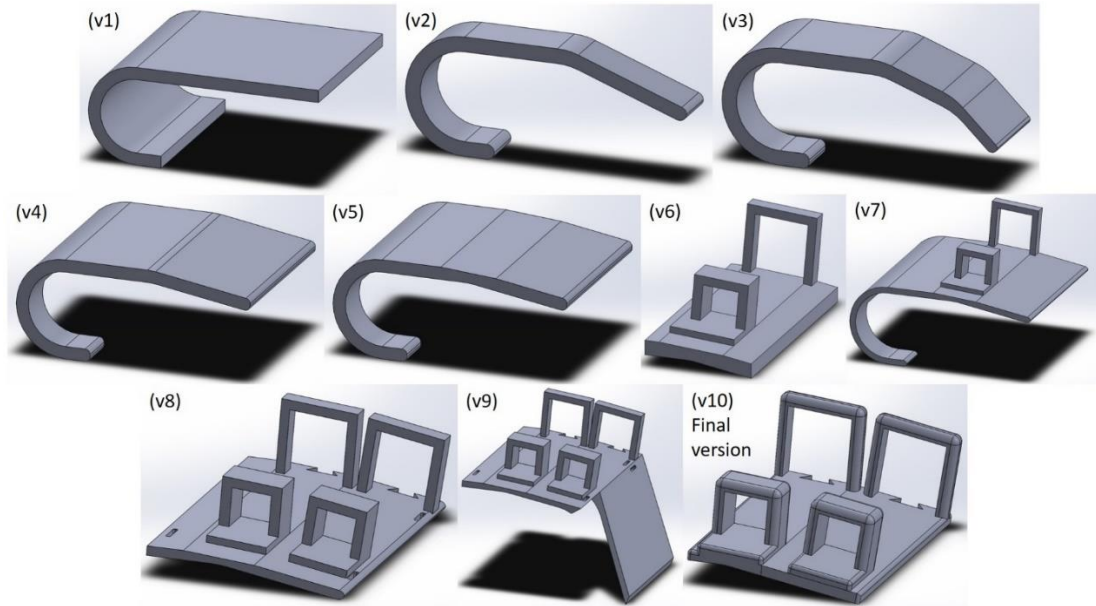


Figure A.2 Design iterations of the thumb actuator mount.

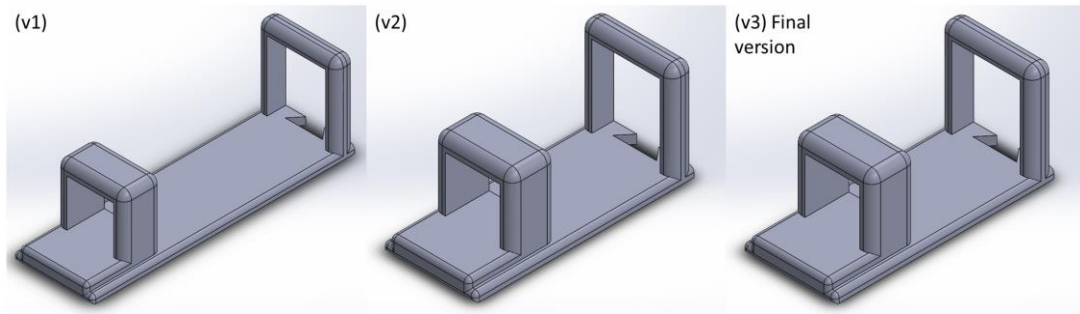


Figure A.3 Design iterations of the thimbles. Model v3 was used in the initial feasibility test.

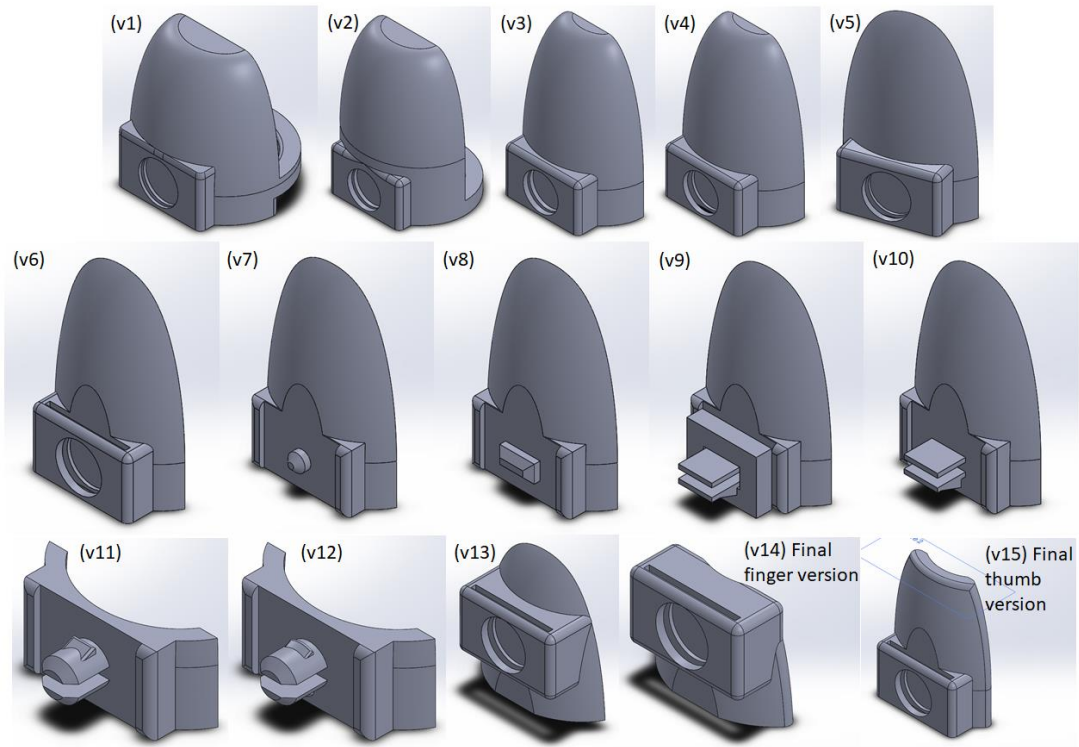


Figure A.4 Design iterations of the control system box.

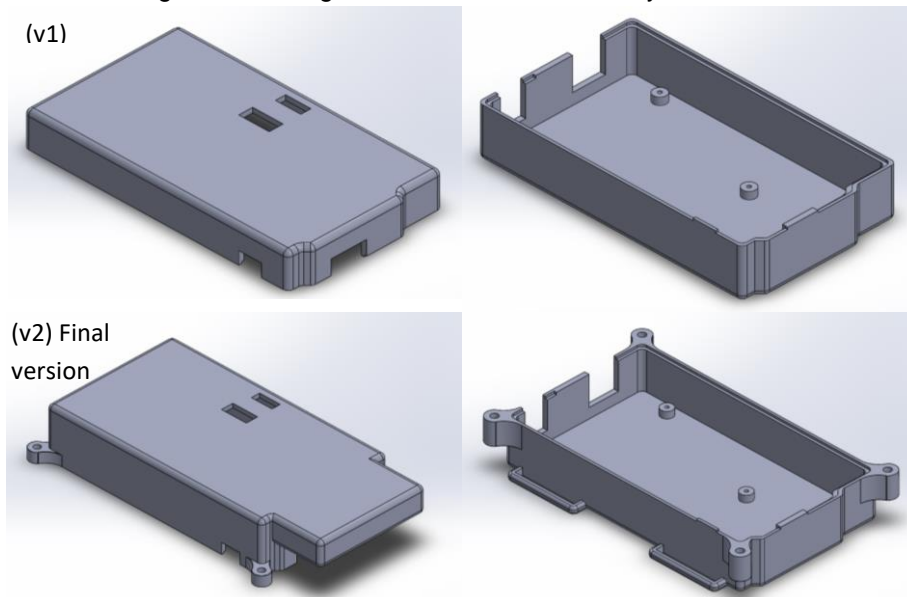
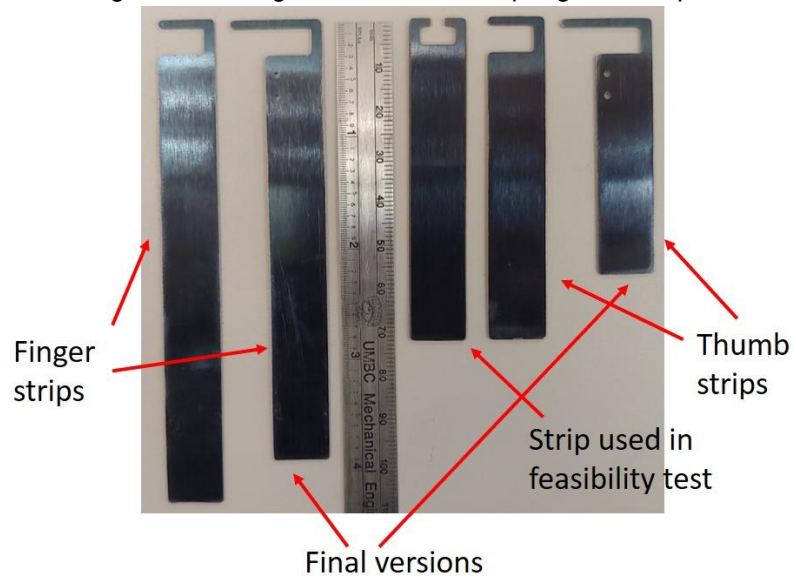


Figure A.5 Design iterations of the spring steel strips.



BIOGRAPHY OF THE AUTHOR

Daniel Chizhik was born and raised in Baltimore, Maryland. He graduated from high school in 2016. He attended the University of Maryland, Baltimore County and graduated in 2018 with a Bachelor's degree in Mechanical Engineering. He moved to Maine and entered the Mechanical Engineering graduate program at the University of Maine in the summer of 2018. Daniel is a candidate for the Master of Science degree in Mechanical Engineering from the University of Maine in May 2020.